Materials with giant mechanocaloric effects: Cooling by strength

Lluís Mañosa and Antoni Planes

Departament de Física de la Matèria Condensada,

Facultat de Física, Universitat de Barcelona,

Martí i Franquès, 1, E-08028 Barcelona. Catalonia.

(Dated: September 13, 2016)

Abstract

The search for materials with large caloric effects has become a major challenge in material science due to their potential in developing near room-temperature solid-state cooling devices, which are both efficient and clean, and that can successfully replace present refrigeration technologies. There are three main families of caloric materials: magnetocaloric, electrocaloric and mechanocaloric. While magnetocaloric and electrocaloric materials have been studied intensively in the last few decades, mechanocaloric materials are only very recently receiving a great deal of attention. The mechanocaloric effect refers to the reversible thermal response of a solid when subjected to an external mechanical field, and encompasses both the elastocaloric effect, corresponding to a uniaxial force, and the barocaloric effect, which corresponds to the response to hydrostatic pressure. In the present paper we review the state of the art in giant mechanocaloric effects and we provide a critical analysis of the thermodynamic quantities that characterize the major families of barocaloric and elastocaloric materials. We finally provide our perspectives for further development in this area.

I. INTRODUCTION

Conventional refrigeration devices are nowadays based to a very large extent on vapor compression technology, which consists of compressing and expanding a fluid within its liquid-vapor coexistence region. This is an old technology that has been highly optimized during recent decades, but which has a considerable environmental impact. Such an impact is due to the fact that the best refrigerant fluids are either toxic (ammonia-based chemicals are still being used for industrial refrigeration) or produce ozone depleting and/or greenhouse effects (CFC and HFC fluids). Therefore, there is an urgent need to replace this technology with a clean, environmentally friendly one, especially after the new global climate Paris agreement[1].

In fluid compression technology, cooling occurs during the evaporation process induced by fast expansion. Solids are usually very incompressible and mechanically induced temperature changes are, in general, very small and thermal effects are only expected to be reasonably significant in systems that can support large reversible deformations. This has been known to happen in materials such as rubber[2] for a very long time and more recently a large thermal response has been reported to occur in superelastic martensitic materials[3]. This thermal response proves that superelastic materials diplay mechanocaloric properties that share numerous similarities with the well-known magnetocaloric effect in magnetic materials. Actually, the magnetocaloric effect refers to the reversible thermal response of any magnetic material under application or removal of an external applied magnetic field. The magnetocaloric effect has been studied for almost one century, first in paramagnetic salts with the aim of reaching near absolute zero temperatures[4,5], and later, after the seminal work of Brown using Gd[6] and especially after the discovery of the giant Gd-Si-Ge magnetocaloric material[7], it was further studied in order to develop materials for room temperature magnetic-refrigeration applications as an alternative to vapor-compression technology. Recently, the mechanocaloric effect together with other caloric effects such as the electrocaloric effect have also attracted a lot of interest and materials displaying a large caloric response have been developed[8,9]. At present, it is acknowledged that solid-state refrigeration technologies based on these caloric effects will be given priority so as to reduce wasting energy for home refrigeration, and to minimize ozone depleting and greenhouse chemicals that seem unavoidable in present vapor-compression technologies.

There are a number of good review papers dealing with magneto-[10–13] and electrocaloric[14,15] materials, but at present there is a lack of deatiled comprehensive review papers that summarize the state-of-the-art in mechanocaloric materials, and only brief reports have been published until now[16,17]. The present paper aims to fill this gap by dealing with recent progress in the development of mechanocaloric materials. Among these materials, pure ferroelastic materials and more specifically, thermoelastic martensitic alloys are, at present, among those with expected optimal mechanocaloric performance. This is associated with superelastic behavior together with excellent mechanical properties, combined with easy availability of the constitutive elements, which suggests long-life operation. In fact, the U.S. Department of Energy has recently acknowledged that thermoelastic cooling technologies based on the use of this class of materials has the highest potential when compared with many other technologies for near room-temperature refrigeration applications[18]. In any case, although considerable advances have been made these recent years, overall the research in this field is still in its beginnings and a lot of progress is expected in the near future. Actually, most of the materials reviewed in the present paper, while still showing inferior mechanocaloric performance than thermoelastic materials, reveal an enormous potential, which arises from the fact that in addition to mechanocaloric effects they also display magneto- or eletrocaloric effects due to a strong interplay between structure and polar or magnetic degrees of freedom. Therefore, the combination of the different caloric effects may be a good strategy in order to improve the caloric response of these materials.

II. GENERAL FEATURES OF CALORIC AND MULTICALORIC EFFECTS.

Caloric effects refer to the reversible thermal response of a given material when subjected to changes of an externally applied mechanical, magnetic or electric field. The corresponding caloric effects are the mechanocaloric, magnetocaloric and electrocaloric effects, respectively. In order to quantify such a thermal response the field is usually modified either isothermally or adiabatically. In the first case, a change of entropy of the material occurs, while in the second one, the material responds by changing its temperature. Usually, the field is applied in a given direction, and only its magnitude, y, is varied. The corresponding isothermal and adiabatic response functions are, $\xi_T = (\partial S/\partial y)_T$ and $\xi_S = (\partial T/\partial y)_S$. Taking into account Maxwell relations, it is straightforward to see that $\xi_T = (\partial X/\partial T)_y$ and

$\xi_S = (\partial X/\partial S)_y = -(T/C_y)(\partial X/\partial T)_y$, where X is the projection of the property thermodynamically conjugated to the field y along its direction of application, and C_y is a heat capacity. Note that ξ_T is thus the relevant response function. Changes of entropy and temperature associated with a finite variation of the field are obtained by integration of ξ_T and ξ_S, respectively. In general, caloric effects under field rotation are expected to be very weak. Only in highly anisotropic materials do such effects have any interest. Actually, some recent works[19,20] have shown that materials with high-temperature-dependent magnetic anisotropy display a significant thermal response under magnetic field rotation.

A large caloric response is expected near phase transitions due to the singular behavior of the property X and hence of the entropy. In ferroic materials, such as ferroelastic, ferroelectric and ferromagnetic materials, large caloric effects are expected in the region where the ferroic property spontaneously emerges. Depending on symmetry-dictated conditions and the possible influence of secondary parameters coupled to the ferroic property, the transition can be either continuous or first-order. The latter case is especially interesting since the transition is accompanied by latent heat which provides a high entropy content that can be controlled by an externally applied field[9].

Multiferroics are characterized by two or more ferroic properties. In these materials cross-response to multiple fields is possible[21] and therefore they are susceptible to supporting multicaloric effects, which means that caloric effects associated with each kind of ferroicity may occur in an interdependent manner. The cross-effect is enhanced in these multiferroics where the two (or more) ferroic orders emerge simultaneously and which requires a strong interplay between different ferroicities. Often, this class of materials are classified as multicaloric materials[8]. The themodynamics of multicaloric effects has been developed in detail in Refs. [22 and 23].

In general, the relevant response function ξ_T is negative since ferroic properties such as strain, magnetization and polarization are expected to reach a maximum in the ground state[24]. Thus, materials should warm up when the field is applied and cool down when it is removed. Nevertheless, thermodynamic stability does not impose a particular sign on ξ_T and, actually, in some regions of the space of parameters of a given material ξ_T can be positive. In this case, the material cools down when the field is applied and the caloric effect is denoted as inverse[25]. This anomalous behavior usually occurs in the vicinity of a phase transition and is a consequence of specific features of the interplay between ferroic

properties, or it is associated with frustration effects, or a combination of both[26,27].

III. THERMODYNAMICS

To discuss the thermodynamics of deformable solids under stress, we assume that they can be treated within the continuum approximation. We consider infinitesimal (linear) strains, ε_{ij}, referred to an unstressed configuration and then, in terms of the Cauchy stress σ_{ij}, the following thermodynamic fundamental equation results[28],

$$dU = TdS + V_0\sigma_{ij}d\varepsilon_{ij}, \tag{1}$$

where $U = U(\{\varepsilon_{ij}\}, S)$ is the internal energy; S, the entropy; T, the temperature, and V_0, is the volume of the unstressed solid. Sum over repeated indices is assumed. For the study of mechanocaloric effects it is convenient to take temperature and stresses as independent variables. A Gibbs-like free energy is then introduced via the Legendre transform, $\mathcal{G} = U - TS - V_0\sigma_{ij}\varepsilon_{ij}$. In terms of $\mathcal{G}$, the fundamental equation reads,

$$d\mathcal{G} = -SdT - V_0\varepsilon_{ij}d\sigma_{ij}, \tag{2}$$

from which the following set of Maxwell equation can be derived,

$$\frac{\partial S}{\partial \sigma_{ij}} = V_0\frac{\partial \varepsilon_{ij}}{\partial T}. \tag{3}$$

In the previous equation any temperature dependence of the reference volume V_0 has been assumed negligibly small.

In spite of the fact that the stress has tensorial (rank-2) character, the mechanocaloric effect is usually induced by the change of the magnitude of a given stress-tensor component, or a simple combination of components. For instance, in the two cases of interest in the present paper, elastocaloric and barocaloric effects, thermal changes are induced by the change of magnitude of an uniaxial stress and hydrostatic pressure respectively. In the first case, the stress $\sigma_{ij} = \sigma\delta_{i\mu}\delta_{j\mu}$ is applied along a given direction μ. In this expression δ_{ij} is the Krönecker delta, and $\sigma > 0$ corresponds to an applied tension, while $\sigma < 0$ corresponds to a compression. In the case of the barocaloric effect, $\sigma_{ij} = -p\delta_{ij}$. In both cases the relevant fields (σ or $-p$) can be treated as a scalar. The corresponding response functions quantifying these two mechanocaloric effects are $\xi_{iso} = (\partial S/\partial f)_T$ and $\xi_{adi} = (\partial T/\partial f)_S$, where f is the

scalar field (either σ or $-p$). These two functions are related as, $\xi_{iso} = -C\xi_{adi}/T$, where C is the heat capacity. Strictly, C is the heat capacity at constant force, but since we are dealing with solids we will assume no difference between heat capacity at constant force and heat capacity at constant deformation.

Taking into account the Maxwell relation, in the case of the barocaloric effect ($f = -p$), $\partial S/\partial p = -V_0 \partial\omega/\partial T$, where ω is the volume strain (= Tr $\varepsilon_{ij} = \Delta V/V_0$), while in the case of the elastocaloric effect ($f = \sigma$), $\partial S/\partial\sigma = V_0 \partial\varepsilon/\partial T$, where ε is the deformation along the direction of the applied stress σ. Then for a finite isothermal change of p or σ one obtains the corresponding entropy changes,

$$\Delta S(T, 0 \to -p) = V_0 \int_0^{-p} \left(\frac{\partial\omega}{\partial T}\right)_p dp, \tag{4}$$

$$\Delta S(T, 0 \to \sigma) = V_0 \int_0^{\sigma} \left(\frac{\partial\varepsilon}{\partial T}\right)_\sigma d\sigma. \tag{5}$$

The temperature changes induced by adiabatic variation of p and σ are respectively given by,

$$\Delta T(S, 0 \to -p) = -V_0 \int_0^{-p} \frac{T}{C}\left(\frac{\partial\omega}{\partial T}\right)_p dp, \tag{6}$$

$$\Delta T(S, 0 \to \sigma) = -V_0 \int_0^{\sigma} \frac{T}{C}\left(\frac{\partial\varepsilon}{\partial T}\right)_\sigma d\sigma. \tag{7}$$

Compared to the preceding equations for the entropy change, the computation of ΔT from the present equations is much less straightforward. These equations are in fact transcendental integral equations. When temperature changes are small and the heat capacity can be assumed to be independent of the applied force, to a good approximation,

$$\Delta T(S, 0 \to f = -p, \sigma) \simeq -\frac{T\Delta S(T_i, 0 \to f = -p, \sigma)}{C}, \tag{8}$$

where T_i is the initial temperature of the process.

It is interesting to take into account the fact that usually mechanical experiments aimed at quantifying elastocaloric properties are carried out by controlling strain (or elongation) instead of controlling the uniaxial stress (or applied force). Actually, this is the common procedure followed when measurements are done with standard (screw-driven) tensile machines which enable a very good control of elongation. While in equilibrium both, stress- and strain-controlled measurements should yield exactly the same result, when a first-order phase transition is involved, which necessarily occurs out-of-equilibrium due to unavoidable

nucleation processes, the transition path is known to be influenced by the driving mechanism, even if non-equilibrium effects are weak[29,30]. Therefore, the driving mechanism may affect the computed entropy change in the vicinity of a first-order transition. Actually, the isothermal strain induced entropy change is given by,

$$\Delta S(T, 0 \to \varepsilon) = -\int_0^{\varepsilon} \left(\frac{\partial \sigma}{\partial T}\right)_{\varepsilon} d\varepsilon, \tag{9}$$

where the Maxwell relation $(\partial S/\partial \varepsilon)_T = -(\partial \sigma/\partial T)_{\varepsilon}$ has been taken into account[31]. In practice, the entropy changes obtained as $\Delta S(T, 0 \to \varepsilon)$ and $\Delta S(T, 0 \to \sigma)$ have been found to be the same within errors[29], at least in transitions with weak hysteresis.

Note that even in the simple case of elastic isotropic materials, due to the second-rank tensor nature of stress and strain, a complete characterization of the mechanocaloric effect requires the determination of the caloric responses associated with, at least, dilation and shear deformation modes. Thus, barocaloric and elastocaloric[32] responses provide a full characterization of the mechanocaloric effect in elastic isotropic materials. As an example, let us assume that the deformation is given by the sum of a pure dilation, ω, plus a pure shear of magnitude ϵ, so that $\varepsilon_{xx} = \omega/3+\epsilon$, $\varepsilon_{yy} = \omega/3-\epsilon$, $\varepsilon_{zz} = \omega/3$, and the non-diagonal elements $\varepsilon_{i\neq j} = 0$. It is then easy to obtain that for the barocaloric effect $\xi_{iso}^{bar} = -\partial\omega/\partial T$, and for the elastocaloric effect associated with an applied uniaxial stress along the x-direction, $\xi_{iso}^{elas} = \partial(\omega/3 + \epsilon)/\partial T$. It is interesting to note that if the deformation is dominated by a pure shear, the barocaloric effect will vanish. However, if it is dominated by a pure dilation, both the barocaloric and elastocaloric effects will be related by (assuming $\sigma = -p$),

$$\Delta S(T, 0 \to p) = -3\Delta S(T, 0 \to \sigma = -p). \tag{10}$$

This is expected to be a good approximation near a structural phase transition associated with a pure volume change.

Now let us assume precisely that under an applied force f (uniaxial stress or hydrostatic pressure) the system undergoes a structural phase transition at a temperature T_t. These transitions are characterized by a sharp change of the corresponding conjugated strain variable λ (ε or ω). In general, it can be assumed that λ shows the following behavior close to the phase transition,

$$\lambda(T, f) = \lambda_0(T, f) + \Delta\lambda\mathcal{H}[(T_t(f) - T)/\delta T], \tag{11}$$

where $\mathcal{H}$ is a shape-function that varies from 0 to 1 within the region δT, which represents a measure of the temperature range over which the transition spreads in temperature. In the limit $\delta T \to 0$, $\mathcal{H}$ approaches a Heaviside function, which describes the expected discontinuous behavior of a first-order transition. The change of entropy induced by an isothermal change of f, can then be computed as,

$$\Delta S(0 \to f) = \int_0^f \left(\frac{\partial \lambda}{\partial T}\right)_f df = \begin{cases} -\frac{\Delta\lambda}{\alpha} & \text{for } T \in [T_t(0), T_t(f)] \\ 0 & \text{for } T \notin [T_t(0), T_t(f)] \end{cases}, \tag{12}$$

where we have taken into account that $\left(\frac{\partial \lambda}{\partial T}\right)_f$ is the Dirac δ-function, and we have assumed that λ_0 and $\Delta\lambda$ are independent of temperature. In the preceding equation $\alpha = dT_t/df$ is also assumed constant. Note that in spite of the fact that $(\partial\lambda/\partial T)_f$ diverges at the transition, the obtained change of entropy is well defined. In fact, the preceding calculation shows that integration of the Maxwell relation $(\partial S/\partial f)_T = (\partial\lambda/\partial T)_f$ in the vicinity of the transition discontinuity renders, as expected, the Clausius-Clapeyron equation, $dT_t/df = -\Delta\lambda/\Delta S$.

The Clausius-Clapeyron equation can be applied to evaluate both barocaloric and elastocaloric effects close to first order transitions. Actually, this equation provides the contribution to the field induced entropy change solely associated with the phase transition. Therefore, when this method is used, the contribution arising from any intrinsic temperature dependence of the property λ (volume in the case of the barocaloric effect ant strain in the case of the elastocaloric effect) outside the transition is not taken into account. As these contributions may be of opposite nature to the contribution associated with the transition (either conventional or inverse), the final entropy change can be larger (when all contributions are of the same nature) or smaller (when they are of opposite nature) than the entropy change estimated from Maxwell relations (eqs. 4 and 5) even if the applied field is large enough to ensure that the whole transition is induced.

Close to a phase transition, eq. 8 represents, in principle, too crude an approximation. In this case, one can proceed by assuming that the entropy can be expressed as the sum of a background (or non-singular) term (associated, for instance, with lattice vibrations), S_{vib}, which can be assumed to depend only on temperature, plus a singular term, S_{sin}, that brings in the field dependence. Then, for an adiabatic (reversible) change of the field, since the total entropy must remain constant, $S_{vib}(T_f) - S_{vib}(T_i) = -[S_{sin}(T_f, f) - S_{sin}(T_i, f = 0)]$, where T_i and T_f are the initial and final temperatures of the process. Assuming that

$S_{vib}(T_f) - S_{vib}(T_i) \simeq C_{vib} \ln(T_f/T_i)$, the following is obtained,

$$T_f = T_i \exp\left\{-\frac{1}{C_{vib}}[S_{sin}(T_f, f) - S_{sin}(T_i, f = 0)]\right\}. \quad (13)$$

This equation clarifies the relevance of the heat capacity on the temperature change induced by adiabatic application/removal of an external field (see eqs.6 and 7). According to eq. 13, this change is controlled to a large extent by the vibrational contribution to the heat capacity, which is expected to weakly depend on both temperature and applied field, at least at high enough temperatures, which is the range of interest in the present paper.

Taking into account the fact that close to room temperature $C_{vib} \simeq 3R$ is typically one order of magnitude larger than $S_{sin}(T_f, f) - S_{sin}(T_i, f = 0)$, which is bounded by the transition entropy change, expanding the exponential one obtains,

$$\Delta T(S, 0 \rightarrow y) = T_f - T_i \simeq -\frac{T_i}{3R}[S_{sin}(T_f, f) - S_{sin}(T_i, f = 0)] + ... \quad (14)$$

To a first order of approximation, the obtained result is similar to the previous eq. 8, but now $C = 3R$ is the high temperature vibrational heat capacity, and ΔS is the entropy change associated with the transition (which as we will see can be obtained experimentally from calorimetric experiments).

It is worth noting that near a sharp first-order phase transition $\Delta T(S, 0 \rightarrow f)$ should coincide with the shift of transition temperature induced by the applied field, $\Delta T_t(f)$. However, in real materials first-order phase transitions are not sharp, and the transition is spread over a certain temperature interval. Strictly speaking this is a non-equilibrium effect that can be explained by taking into account a number of factors including the existence of composition gradients, lattice defects, etc... In the case of transitions that involve a structural change, the temperature spread is to a large extent a consequence of the fringing elastic fields due to strain matching conditions induced by the transformation symmetry change[33,34]. In this case, it has been shown that the change of temperature induced by adiabatic application of a field should be lower than the corresponding shift of transition temperature. The difference depends on the slopes of the entropy versus temperature curve outside and within the transition region[35].

Non-equilibrium effects are unavoidable when dealing with first-order transitions. The existence of hysteresis is the main consequence of the fact that the transition path occurs out-of-equilibrium. As regards caloric effects, this is important since hysteresis imposes serious limitations to the reversibility of caloric effects upon successive field cycling. At present,

it is well known that the reversibility of any caloric effect depends essentially on the competition between the temperature width of the hysteresis and the temperature-shift of the whole hysteresis loop due to the applied field. Indeed, narrow hysteresis favors reversibility. On the other hand, even if the hysteresis is large, a strong temperature shift of the characteristic forward and reverse transition temperatures would also lead to substantial reversibility. In systems showing a conventional caloric effect, reversible values for the field-induced adiabatic temperature and isothermal entropy changes are found within a temperature interval bounded by the start temperature of the transition on cooling at zero applied field and the start temperature of the subsequent transition on heating under an applied field. Instead, this interval is bounded by the start transition temperature on heating at zero field and the transition temperature on cooling under an applied field when the caloric effect is inverse[36]. In both cases, in the reversible temperature region, the field carries the state of the material through a minor hysteresis loop, and the reversibility of the caloric effect is directly related to the reversibility in the fraction of material that undergoes the transition on cooling and on subsequent heating in the cycle[37]. Indeed, when the size of the transition shift due to the applied field is large enough, these minor loops will approach the full transformation loop and the caloric effect will become reversible from cycle to cycle.

IV. MEASUREMENT TECHNIQUES

As discussed in the previous sections, mechanocaloric effects are typically characterized by the isothermal entropy change (ΔS) and the adiabatic temperature change (ΔT) associated with the application (or removal) of an external stress. The values of these quantities can be obtained from experiments by a variety of measurement protocols which are broadly classed into indirect, quasi-direct and direct methods[9,36]. As will be seen in the following, in the analysis of caloric effects it is important to specify the experimental method used in determining caloric quantities because data obtained from different methods do not always coincide. It is worth noticing that although hydrostatic pressure corresponds to a negative value of the stress tensor components, in experimental data, positive values correspond to application of pressure. These criteria will also be used in the following.

Indirect methods involve the measurement of the temperature and stress dependence of the strain and rely on the use of the Maxwell relations (see equations 4-7). Indirect methods are

the most popular ones in the study of magnetocaloric and electrocaloric effects because both magnetization and polarization are readily measurable to a high accuracy. In the case of the barocaloric effect, volume changes are usually small even across structural transitions and it is challenging to measure them as a function of both temperature and pressure with enough accuracy to numerically compute entropy changes. On the other hand, for elastocaloric materials, length changes across the transition can be measured by suitable strain gauges. The entropy change is then computed by eq. 5 which, expressed as specific entropy (*i.e.* per unit mass) reads:

$$\Delta S^i = \frac{1}{\rho}\int_0^\sigma \left(\frac{\partial \varepsilon}{\partial T}\right)_\sigma d\sigma = \frac{1}{m}\int_0^F \left(\frac{\partial L}{\partial T}\right)_F dF \tag{15}$$

where ρ is the mass density, F is the applied uniaxial load, and m and L are, respectively, the mass and the gauge length of the specimen. $\sigma = F/A$ (with A the cross section which is assumed to be constant) and $\varepsilon = (L - L_0)/L_0$ (where L_0 is the gauge length at zero stress, which is taken as constant).

Quasi-direct methods are based on calorimetric measurements under external applied fields, and for first-order phase transitions, differential scanning calorimety (DSC) under applied external fields is the most suitable technique. In this case, DSC heating and cooling runs are performed at different (constant) values of the applied external field (stress). These kinds of calorimeters are available in the case of barocaloric studies (DSC under hydrostatic pressure) but, at present, no suitable DSC has been reported to our knowledge that can operate under uniaxial external loads. Data from DSC under an applied field are complemented with specific heat (C) data on each phase away from the structural transition (which extends from T_1 to T_2) and under the assumption that in these regions C is not significantly influenced by pressure. The entropy (referenced to the value at a given temperature T_0) for a heating run is then computed as:

$$S(T,p) = \begin{cases} \displaystyle\int_{T_0}^{T} \frac{C^L}{T} dT & T \le T_1 \\ \displaystyle S(T_1,p) + \int_{T_1}^{T} \frac{1}{T}\left(C + \frac{dQ}{dT}\right) dT & T_1 < T \le T_2 \\ \displaystyle S(T_2,p) + \int_{T_2}^{T} \frac{C^H}{T} dT & T_2 < T \end{cases} \tag{16}$$

where $\frac{dQ}{dT} = \frac{\dot{Q}}{\dot{T}}$ with $\dot{Q}$ being the heat flux measured by DSC and $\dot{T}$, the heating rate. C^L and C^H are, respectively, the specific heat of the low and high temperature phases and $C = xC^L + (1-x)C^H$ where x is the fraction in the low temperature phase. Frequently, within the transition region, $C \simeq C^L \simeq C^H$. By an appropriate change of the integration limits, an equivalent expression is used for cooling runs.

The entropy change associated with the application of a pressure p is obtained by subtracting the $S(T,p)$ curves:

$$\Delta S^{qd} = S(T,p) - S(T,0) \tag{17}$$

(where $p = 0$ refers to atmospheric pressure). On the other hand, the temperature change can be obtained by subtracting the corresponding $T(S,p)$ curves:

$$\Delta T^{qd} = T(S,p) - T(S,0) \tag{18}$$

Direct methods in the determination of entropy changes require the use of DSC's under an applied field that can operate isothermally while the field is scanned. This kind of calorimetry has been successfully applied to the study of magnetocaloric[36,38] and electrocaloric[39] effects. However, until now this technique is not available for the study of mechanocaloric effects. On the other hand, direct measurements of adiabatic temperature changes (ΔT^d) can be performed by suitable thermometers attached to the studied sample or alternatively by means of non-contact infrared thermometry. The adiabaticity of these measurements relies on the ratio between the characteristic time constant associated with the application (or removal) of stress and the time constant associated with the heat exchange between sample and surroundings. In the case of barocaloric effects, the sample is surrounded by a pressure transmitting fluid and measurements are not fully adiabatic thereby leading to measured ΔT^d values which are typically underestimated. However in typical elastocaloric experiments the sample is in air, and application (or removal) of uniaxial stresses at strain rates greater than 0.1 s^{-1} have proved to be close to the adiabatic limit and have provided reliable data for the adiabatic temperature change.

It is also worth mentioning that it is customary to estimate temperature changes from measured entropy changes (or alternatively entropy changes from measured temperature data) by means of equation 8 but, as previously mentioned this is a crude approximation

which typically provides data which are overestimated for ΔT^e and underestimated for ΔS^e

V. MECHANOCALORIC MATERIALS.

Giant values for the mechanocaloric quantities require that some of the strain-tensor components experience large changes over a narrow temperature domain. This situation typically occurs at a first-order structural transition, and therefore most materials with giant mechanocaloric effects undergo a structural transition which encompasses a modification in the crystal unit cell.

Depending on the structural distortion at the phase transition, giant mechanocaloric materials can be broadly classed into different groups, as shown in Figure 1. The lattice distortion can be accounted for by a pure dilation, a pure shear or a combination of both. Furthermore, in magnetic and polar materials, there can be an interplay between structural, magnetic and polar degrees of freedom and transitions can also encompass changes in magnetization and polarization in addition to the structural changes. While no giant mechanocaloric materials have been reported so far with a purely dilational structural transition, conventional shape-memory alloys (SMA) represent prototype ferroelastic materials where the lattice distortion is a pure shear strain. On the other hand, most giant magnetocaloric and electrocaloric materials undergo first-order phase transitions involving changes in the crystal unit cell. In most cases these distortions involve both shear and dilation strains. However, for some magnetic shape memory alloys, the volume change is very small. In addition for selected magnetocaloric materials where there is no change in the crystal symmetry at the magneto-structural transition, there is an isotropic expansion (or compression) of the lattice giving rise to a pure dilation strain (volume change).

A salient feature of non-magnetic SMA is that they have excellent mechanical properties (very good ductility) in contrast to magnetic and polar materials which are brittle (with the exception of Fe-based magnetic alloys). Hence SMA can support large uniaxial stresses and therefore are the best candidates for elastocaloric purposes. In contrast, most studies in magneto-structural and electro-structural materials have been performed under hydrostatic pressure because material brittleness is not such a crucial issue in this case. For these alloys, uniaxial stress measurements have only been conducted in magnetic shape-memory and Fe-based alloys.

In the following sections we will survey the most relevant physical properties of these mechanocaloric materials and results are compiled in tables 1 and 2.

VI. MATERIALS WITH PURELY STRUCTURAL TRANSITIONS.

Prototype materials with giant mechanocaloric effects associated with a purely structural transition are non-magnetic shape memory alloys (SMA). These alloys undergo a martensitic transition from a high temperature cubic structure towards a low temperature lower symmetry phase. The martensitic transition is first-order, difusionless, and the lattice distortion is basically described by a shear of the $\{110\}$ planes along the $< 1\bar{1}0 >$ directions. This class of alloys have received a great deal of attention for many decades owing to their unique thermo-mechanical properties they exhibit such as pseudoelasticity, superelasticity and shape memory[40].

Because the lattice distortion at the transition is a pure shear, the martensitic transition in these alloys is rather insensitive to hydrostatic pressure, and SMA do not exhibit significant barocaloric effects. On the other hand, the shear distortion is considerably larger (with values that can reach more than 10%), which results in a strong sensitivity of the martensitic transition to the application of uniaxial stress. Such a strong sensitivity added to the large latent heat of the martensitic transition confer excellent elastocaloric properties to these alloys. There are a variety of SMA, and giant elastocaloric effects have been reported for Cu-based and Ni-Ti-based families of alloys.

The high temperature phase of these alloys (usually known as austenite) is an open bcc-based cubic structure. Such a structure is easily deformable by shearing the $\{110\}$ planes, and the energy of the phonon modes associated with such a distortion (TA_2 branch) as well as the associated elastic constant C' have very low values. These low-energy phonon modes have a two-fold role in the phase stability of SMA. On the one hand, the cubic phase has incipient mechanical instability for $\{110\} < 1\bar{1}0 >$ shears that bring the system towards the martensitic phase. On the other hand, there is a large vibrational entropy arising from these low-energy TA_2 phonons, which is the main factor that stabilizes the cubic phase at high temperatures. Hence, the entropy change at the martensitic phase transition has a predominantly vibrational origin[41]. The contribution from conduction electrons does not play a relevant role in Cu-based alloys[42], but it can become relevant for Ni-Ti[43].

The high temperature phase of Cu-based alloys is an ordered cubic ($Fm3m$) structure (DO_3 and $L2_1$ type of order depending on composition) which transforms to a monoclinic phase ($C/2m$). The monoclinic unit cell is rarely used to describe martensite and larger higher symmetry unit cells are commonly used instead to describe the different martensitic structures. Typically these are orthorhombic ($I2/m$) and hexagonal ($Pnmm$) cells. Common martensitic structures in Cu-based alloys are 3R, 6R, 9R, 18R and 2H where R refers to orthorhombic and H to hexagonal, and the number indicates the periodicity in the modulation of the close-packed planes[44].

The first studies of the elastocaloric effect in Cu-based alloys were performed on a Cu-Zn-Al single crystal subjected to uniaxial tensile stresses along the [100] direction[29]. The isothermal entropy change was computed using equation 15 from the stress-strain curves recorded at selected temperatures and the maximum obtained value for stresses around 100 MPa was $\Delta S^i \simeq 21$ Jkg^{-1}K^{-1}, which coincided with the transition entropy change ΔS_t. It was also proved that the energy dissipated in a complete transformation loop was weak in comparison to the latent heat of the transition[45].

The adiabatic temperature changes were measured on a different single crystalline sample with close composition, by means of infrared thermal imaging[46]. The obtained values ($\Delta T^d \simeq 6$ K) were lower than those expected from the entropy change, where the discrepancy was due to the short gauge length of the sample which resulted in heat leakage through the grips. Studies on longer samples rendered ΔT^d values ($\sim$ 10-14 K) in agreement with the estimations from the entropy data[3,47]. Infrared images revealed markedly non-uniform temperature profiles. Actually, the measured temperature footprints matched the development of a single martensitic variant predicted by crystallographic theory. Furthermore, the evolution of these profiles proved to be an excellent tool to follow the kinetics of the martensitic transition (nucleation and subsequent growth) which takes place by a process of avalanches[48].

In view of possible applications in refrigeration, the temperature span over which large (giant) ΔS and ΔT values can be found limits the operation temperature range of a future device. In a later study on a Cu-Zn-Al polycrystal[49] it was found that the elastocaloric effect in Cu-based alloys spans over a very large temperature range ($\sim$ 130 K) which is bounded at low temperatures by the stress-free transition temperature and at high temperatures by the critical resolved stress for plastic deformation. Such a large temperature span results in

an outstanding refrigerating cooling power RCP [10], of 2300 Jkg^{-1}.

Compression tests were also perfomed on a Cu-Zn-Al single crystal[50]. In this case, the strain was measured at a constant stress while temperature was continuously swept. Results are comparable to those obtained in tensile experiments. A typical feature for Cu-based alloys is that the maximum transition strain (ε) is achieved at very low values of the applied stress, in contrast to other martensitic materials for which ε monotonously increases with increasing stress and the maximum value is only achieved at high stress values. This peculiarity along with the strong sensitivity of the transition temperature to applied stress ($dT/d\sigma \simeq 0.5$ KMa^{-1}), result in excellent reproducibility of the elastocaloric effect upon stress cycling (even at low values of the applied stress)[49].

Ni-Ti alloys transform martensitically for compositions very close to the stoichiometric 50-50 structure. In these alloys, the high temperature phase is an ordered ($B2$ or $CsCl$ order) cubic phase ($Pm3m$). The martensitic phase is monoclinic, and is denoted as B19' ($P2/m$). However, depending on heat treatment and doping elements the martensitic transition occurs via intermediate structural phases[51]. Hence, for suitably annealed samples, the cubic structure transforms towards a trigonal R phase ($P3$) which upon further cooling transforms towards the B19' phase. On the other hand, in Cu-doped samples (with Cu $\geq$ 5%), the B2 phase transforms towards an orthorhombic martensite ($Pmma$) which is denoted as B19.

The Ni-Ti family of alloys are the most studied mechanocaloric compounds so far. An early study of the possibilities of this alloy for cooling purposes was already reported in ref. [52]. Below we will discuss some of the most relevant findings that have come out of recent studies.

As regards the B2 $\leftrightarrow$ B19' transition, the sensitivity of the transition temperature to stress is relatively low in the range 0.120-0.2 KMPa^{-1}, and the transition occurs with significantly large hysteresis. As a result of these features, large stresses are required to obtain significant elastocaloric effects associated with this transition in Ni-Ti alloys. On the other hand, however, this transition shows a very large transition entropy change (ΔS_t) which results in very high values for the corresponding elastocaloric ΔT and ΔS (for high enough applied stresses). It is also worth noting that ΔS_t values are sensitive to the heat treatment and doping elements and values listed in Table 1 for different alloys span a broad range.

Tensile experiments were conducted on a $Ni_{50.38}Ti_{49.62}$ single crystal along different crys-

tallographic directions[53]. Upon stress, the sample transformed from the B2 to the B19', and the best results were obtained when the stress was applied along the [1 4 8] direction. For applied stresses up to 500 MPa, the measured adiabatic temperature change was $\Delta T^d \simeq 15$ K, which is a value lower than the maximum expected value computed from the entropy change of the transition. Larger ΔT^d values were measured on polycrystalline wires[54,55] for slightly larger stress values. In this case, the stress to induce the transition using tension was lower than with compression, but compression tests had the advantage of showing a lower hysteresis and better fatigue properties because of lower crack mobility under compression than under tension.

Infrared measurements on foil specimens[56–58] revealed very inhomogeneous temperature contour maps, with patterns that matched the development of martensitic variants, similarly to what was reported for Cu-based alloys. It is noticeable the particularly large $\Delta T^d \simeq 58$ K measured for a foil stressed up to 1300 MPa[56].

Isothermal entropy changes were determined from strain measurements as a function of temperature under constant applied external load[60]. In contrast to Cu-based alloys, the transformation strain gradually increases with increasing stress. The isothermal entropy change obtained at relatively low stresses ($\sigma = 175$ MPa) is very large ($\Delta S^i \simeq 70$ Jkg^{-1}K^{-1}), and approaches ΔS_t. Nevertheless, it is not expected that these values are reproducible upon successive stress cycling of the sample due to large hysteresis.

It is well known that the properties of the B2 $\leftrightarrow$ B19' transition evolve upon cycling. Particularly, the latent heat of the transition has been found to decrease (15-25 % reduction) after approximately one hundred training cycles[61]. Such an evolution also affects elastocaloric performance and indeed significantly lower values for ΔT and ΔS are obtained in samples that have been trained for several cycles[55].

Within a certain range of compositions and by suitable heat treatments, Ni-Ti alloys are reported to behave as strain glasses[62]. Studies on a $Ni_{48.7}Ti_{51.3}$ containing Ti_3Ni_4 nanoprecipitates subjected to tensile stresses[63] showed that at low stress level (≤ 130 MPa) the sample exhibits a strain glass transition, whereas at higher stresses the B19' phase is induced. There is a tiny elastocaloric effect at the glass transition ($\Delta S^i \simeq 1.3$ Jkg^{-1}K^{-1} for $\sigma = 150$ MPa), while the transition to B19' phase exhibited values comparable to those of samples without nano-precipitates ($\Delta S^i \simeq 26$ Jkg^{-1}K^{-1} at $\sigma = 300$ MPa).

The effect of doping elements on the elastocaloric properties of Ni-Ti based shape memory

alloys was also investigated. In a $Ni_{50.5}Ti_{49.1}Fe_{0.4}$ foil annealed at 773 K, the martensitic transition occurred in a two-step process via the intermediate R phase, and the measured adiabatic temperature change was $\Delta T^d \simeq 17$ K at 500 MPa[59]. When the sample was annealed at 723K , the B2 $\leftrightarrow$ B19' transition occurred in a single step, with a latent heat of about half that of the two-step transformation. Based on an extensive study of more than 70 alloy compositons, a quaternary $Ni_{45}Ti_{47.25}Cu_5V_{2.75}$ was selected to exhibit a good elastocaloric performance[61]. Adiabatic temperature changes of $\Delta T^d \simeq 8$ K were measured at σ= 500 MPa. These values were found to be reproducible once the sample had been subjected to several training cycles.

Very promising alloys are Cu-doped Ni-Ti alloys with Cu compositions above 5% [Refs. 64 and 65]. In these alloys the martensitic transformation takes place, in a single step, from the cubic B2 phase to the othorhombic B19 phase. Although the transition entropy change is slightly lower than for the B2 $\leftrightarrow$ B19' transition with typical values in the range $\Delta S_t \sim$ 30-60 $Jkg^{-1}K^{-1}$, the critical stress to induce the transition and hysteresis are significantly lower. Direct measurements of adiabatic temperature changes in Cu-doped Ni-Ti films have rendered values in the range $\Delta T^d \sim$ 6-10 K, for tensile stresses of $\sigma \sim$ 200-300 MPa. The isothermal entropy change derived from stress-strain curves is relatively large ($\Delta S^i \simeq 40$ $Jkg^{-1}K^{-1}$). A unique property of Ni-Ti-based alloys undergoing a B2 $\leftrightarrow$ B19 transition is the excellent reproducibility in both ΔT and ΔS values in many cycles. Actually, these alloys exhibit ultra-low fatigue[66], and it has recently been demostrated that cycling the alloys through the B2 $\leftrightarrow$ B19 transition for more than 10 million cycles did not produce any noticeable change in the characteristics of the transformation. Such an enhanced stability occurs in the Ti-rich compositional range and it is associated with the growth of Ti_2Cu precipitates. These precipitates are epitaxially related to the B2 and B19 phases thereby reducing misfits in the lattice parameters at the phase transformation which result in a low fatigue state.

The elastocaloric properties associated with the B2 $\leftrightarrow$ R transition have also been studied in a Ni-Ti wire[60]. The transformation strain is small ($\varepsilon \simeq 0.5$ %), which results in a weak dependence of the transition temperature upon stress. However, the stress required to induce the transition is quite low and moderate values for the entropy change ($\Delta S^i \simeq 13$ $Jkg^{-1}K^{-1}$) have been obtained for stresses $\sigma \sim$ 0.1-0.2 GPa. An interesting property of these transitions is the reduced hysteresis which ensures that these ΔS values are reproducible under cycling

the sample at low stress values. It is also expected that the samples will exhibit good fatigue behavior when cycled across the B2 $\leftrightarrow$ R transition (provided that the B19' phase is avoided).

Interestingly, inverse elastocaloric effects have been reported in $Ni_{51}Ti_{49}$ samples containing aligned coherent particles of Ti_3Ni_4 precipitates[67]. The internal stresses created by these precipitates promote a reverse martensitic transition (from the R phase to the B2 phase) when an external uniaxial stress is applied in a direction perpendicular to the internal stress. Such a reverse transition results in an adiabatic temperature decrease $\Delta T^d \simeq 1.1$ K under the application of a $\sigma \simeq 340$ MPa. Further increase of the stress result in a conventional elastocaloric effect.

VII. MATERIALS WITH MAGNETO-STRUCTURAL TRANSITIONS

Giant magnetocaloric effects are usually related to magnetic transitions which are first-order. For these transitions, in addition to the change in magnetic order, there is also a change in the crystal structure, and therefore most giant magnetocaloric materials are also prone to exhibit giant mechanocaloric properties. Magnetization and strain are the ferroic properties for these magneto-structural transitions, and they are associated with the order parameters of the transition. These two order parameters are typically coupled, and the cross-response of the material to the external stimuli (magnetic field and stress) depends on the strength of such a coupling.

The structural changes at a magneto-structural transition can either involve changes in the crystal symmetry of the material, or alternatively be a uniform expansion (or contraction) of the unit cell where the crystal symmetry remains unaltered. In the latter case, the transition is also known as a magnetoelastic transition. The two cases will be considered in the following sub-sections.

A. Transitions without changes in crystal symmetry

As discussed in section III a uniform change in the unit cell (dilation strain) will give rise to both elastocaloric and barocaloric effects, the latter being dominant. While there are a variety of magnetocaloric materials undergoing purely magnetoelastic transition, mechanocaloric

effects have only been reported for a few of them and these are discussed below.

Fe-Rh alloys with composition close to the stoichiometric FeRh undergo a magneto-structural transition from a high temperature ferromagnetic (FM) phase towards a low temperature antiferromagnetic (AFM) state. The crystal structure is $CsCl$ cubic ($Pm3m$), with the volume of the AFM phase lower than that of the FM volume ($\Delta v/v \sim 1\%$). In the FM state, Fe atoms have a $\sim 3\ \mu_B$ moment and Rh atoms $\sim 1\ \mu_B$, while in the AFM state there is no appreciable magnetic moment in the Rh atoms, while the Fe atoms have $\sim 3\ \mu_B$ with opposite signs on successive layers of (111) iron planes[68]. The entropy change at the phase transition is in the range $\Delta S_t \sim$ 10-13 Jkg^{-1}K^{-1} depending on composition and heat treatment, and contains contributions from magnetic, electron and vibrational degrees of freedom. Although the weight of each contribution in the relative stability of the AFM and FM phases is still a subject of active debate[69–71], there is general agreement that the vibrational contribution is larger in the low temperature AFM phase while both magnetic and electron contributions are lower in the AFM than in the FM phase.

Giant magnetocaloric[72] and elastocaloric[73] effects in Fe-Rh were reported in the early nineties, but they received limited interest because it was believed that they were not reproducible. However, it has recently been shown that, in well characterized samples, caloric effects exhibit excellent reproducibility upon field cycling[74–76]. On the other hand, the structural change at the phase transition is a pure dilation, and therefore the sample is expected to exhibit barocaloric effects larger than elastocaloric ones. However, the existence of barocaloric effects in this material was not reported until very recently[74,75].

Calorimetric measurements under hydrostatic pressure were performed on two polycrystalline $Fe_{49}Rh_{51}$ samples. It was found that the transition temperature increased with pressure ($dT/dp \simeq 0.060$ KMPa^{-1}) , in agreement with the fact that pressure stabilises the low volume AFM phase, which gives rise to a conventional barocaloric effect. The corresponding entropy and temperature changes computed from these calorimetric runs were $\Delta S^{qd} \simeq 12$ Jkg^{-1}K^{-1} and $\Delta T^{qd} \simeq 10$ K for applied pressures of 250 MPa. Although the entropy values are moderate, they match the transition entropy values for the magneto-structural transition (ΔS_t) and indeed they can already be achieved at relatively low values of the pressure ($p \simeq$ 100 MPa) which confers a high low-field barocaloric strength to Fe-Rh.

With regards to the elastocaloric effect, early direct measurements of the adiabatic temperature change in polycrystalline $Fe_{49}Rh_{51}$ dumbbell shaped samples subjected to tensile

stresses rendered values $\Delta T^d \simeq$ -5 K for applied stresses $\simeq$ 500 MPa[73]. Interestingly this value corresponds to an inverse elastocaloric effect, in agreement with the decrease in transition temperature with tensile stress ($dT/d\sigma \simeq$ -0.020 KMPa^{-1}). It is worth noticing that this value is around one third of the shift using hydrostatic pressure as expected from a pure dilational strain (see eq. 10). Furthermore, it is also expected that compressional uniaxial stresses will give rise to an increase of the transition temperature with a resulting conventional elastocaloric effect.

An interesting family of materials is the $LaFe_{13-x}Si_x$ and derived quaternary compounds which nowadays are considered as being among the most promising materials for magnetic refrigeration. These alloys crystallize in a cubic $NaZn_{13}$ type structure ($Fm\bar{3}m$) and undergo, on cooling, a first-order magneto-structural transition from a PM to a FM phase. The magneto-structural transition temperature increases with Si content, but the transition changes to second order with the associated decrease in transition entropy change (ΔS_t). It has been found that doping with Co or adding interstitial H also increase the transition temperature to values close to room temperature without a significant loss of the magnetocaloric properties[77]. In both cases the effect of Co or H is to expand the lattice and thus modifies the magnetic exchange coupling between Fe atoms. However, adding H is preferred since the electronic structure of the material is not modified and the hydrides show properties much more similar to those of the parent compounds. In any case, in both cases, the magneto-structural transition also involves an isotropic volume increase $\Delta v/v \sim 1$ % at the PM to FM phase transition.

La-Fe-Si compounds are itinerant ferromagnets, and it has been shown that the development of magnetic order causes changes in the electron and phonon densities of states giving rise to contributions from magnetism, lattice, and electrons to the transition entropy change. These contributions are cooperative (all have the same sign), and result in lower magnetic, electronic and vibrational entropy for the FM, high volume low-temperature phase[78].

The barocaloric effect was reported for a $LaFe_{11.33}Co_{0.47}Si_{1.2}$ compound undergoing a magneto-structural transition at $T_t \simeq 250$ K with a transition entropy change $\Delta S_t \simeq 11$ Jkg^{-1}K^{-1} [79]. The transition temperature was found to decrease with increasing volume ($dT/dp \simeq$ -0.090 KMPa^{-1}), in agreement with the stabilization by pressure of the lower volume high-temperature PM phase. Such a pressure stabilization of the high temperature phase resulted in an inverse barocaloric effect. The isothermal entropy values obtained for

pressures of $\sim$ 200 MPa were moderate $\Delta S^{qd} \simeq 9$ Jkg^{-1}K^{-1}, and slightly lower than the transition entropy change, which indicates that these values of pressure were not high enough to totally induce the magneto-structural transition. Direct measurements of the temperature change confirmed the inverse nature of the barocaloric effect by showing that the sample heated-up upon a fast release of hydrostatic pressure. The obtained values $\Delta T^{d} \simeq 2$ K were markedly lower than the expected ones and the difference was due to a lack of good adiabaticity in the direct measurements.

Giant barocaloric effects have also been reported in Mn_3GaN [80]. This is an itinerant antiferromagnetic system with an antiperovskite unit cell ($Pm\bar{3}m$), which transforms on cooling from a PM phase towards an AFM phase at $T_t \simeq 290$ K. In the AFM phase Mn atoms have a large magnetic moment ($\sim 2\ \mu_B$) which is stabilized by a lattice expansion (the magnetic energy gain in expanding the lattice is larger than the electronic kinetic energy loss). In contrast, in the PM phase, there is a small disordered local moment at the sites of the Mn atoms. This state is stabilized by shrinking the lattice which results in a reduction of the electronic kinetic energy. As a result, there is an isotropic expansion of the unit cell ($\Delta v/v \sim 1\%$) at the magneto-structural transition from the PM to the AFM phases where the volume of the AFM is reduced by magnetic frustration[80]. Specific heat measurements[81] indicated that the main contribution to the transition entropy change is due to magnetic degrees of freedom. The contribution from the lattice has an opposite sign to the magnetic one, and amounts $\sim 10\%$ of the total entropy change, while the electronic contribution was found to be negligibly small.

Calorimetric measurements under hydrostatic pressure have shown that in Mn_3GaN the transition temperature decreases with increasing pressure at a rate $dT/dp \simeq$ -0.065 KMPa^{-1}. Pressure stabilizes the high temperature PM phase with a lower volume and the barocaloric effect is found to be inverse. The isothermal entropy values obtained at $p \simeq 150$ MPa ($\Delta S^{qd} \simeq 22$ Jkg^{-1}K^{-1}) coincide with the transition entropy change indicating that it is possible to drive the AFM to a PM transition for relatively low values of pressure. The measured temperature changes ($\Delta T^{d} \simeq 1.5$ K) do confirm the inverse nature of the barocaloric effect and are lower than those computed using specific heat and calorimetric data ($\Delta T^{qd} \simeq$ 4.5 K), and much lower than the estimated ones using equation 8 ($\Delta T^{e} \simeq 13$ K).

B. Transitions with changes in crystal symmetry

Most magneto-structural transitions encompass a change in the symmetry of the crystal lattice in which the lattice distortion can be described by a combination of shear and dilation strains. Actually, this is the case for the vast majority of materials for which giant magnetocaloric effects have been reported, and up to now mechanocaloric effects have been reported for a few of them.

The prototype magnetocaloric material is the $Gd_5(Si_xGe_{1-x})_4$ system. This compound exhibits a rich phase diagram where the compositions of interest for caloric purposes correspond to the region $0.24 \leq x \leq 0.5$, where it undergoes a transition from a monoclinic ($P112_1/a$) paramagnetic phase to an orthorhombic ($Pnma$) ferromagnetic phase on cooling[10]. The structure is composed of a series of structural slabs ordered perpendicular to the b-axis. At the magneto-structural transition, these slabs are inhomogeneously sheared along the a axis[82]. There is also an expansion of the interslab distance leading to a total volume change $\Delta v/v \sim$ 0.5-1 %. The low temperature orthorhombic (FM) phase has the lower volume and therefore it is stabilized by application of hydrostatic pressure. The shift in the transition temperature with pressure is moderate $dT/dp \simeq 0.035$ KMPa^{-1}.

The transition entropy change at the magneto-structural transition of $Gd_5(Si_xGe_{1-x})_4$ contains contributions from both lattice and magnetic degrees of freedom which add cooperatively. In the Si-rich region of interest here, the values for ΔS_t have been found to decrease when increasing the transition temperature (T_t) independently of the tuning mechanism of T_t (either composition or magnetic field) thereby showing an interesting scaling behavior[83].

Barocaloric effects were studied in the stoichiometric $Gd_5Si_2Ge_2$ compound by means of calorimetry under hydrostatic pressure[84]. The increase in the transition temperature with pressure was consistent with the conventional nature of the barocaloric effect. It was also found that the transition entropy change decreased with increasing pressure at a rate $d\Delta S_t/dp \simeq$ - 0.024 Jkg^{-1}K^{-1}MPa^{-1}. Such a decrease is consistent with pressure shifting the transition temperature towards higher values, and the scaling behavior exhibited by ΔS_t. As regards the barocaloric effect, entropy values at 200 MPa are moderate ($\Delta S^{qd} \simeq$ 11 Jkg^{-1}K^{-1}), slightly lower than the transition entropy change ($\Delta S_t \simeq$ 12 Jkg^{-1}K^{-1}) corresponding to an applied pressure of 200 MPa. On the other hand, direct measurements of the adiabatic temperature change $\Delta T^d \simeq$ 1 K rendered values significantly lower than

those expected from entropy data.

An interesting family of magneto-structural compounds with magnetocaloric properties are the Mn-based ternary compounds with the formula MnTX (T = Ni, Co and X = Si, Ge). In their stoichiometric composition the alloys undergo a second order magnetic phase transition from a paramagnetic to a magnetically ordered state (the particular magnetic order depends on composition), and a structural transition from a high temperature Ni_2In-type hexagonal phase ($P6_3/mmc$) to a low temperature TiNiSi-type orthorhombic structure ($Pnma$) where the hexagonal phase has a smaller unit cell volume than the orthorhombic phase. By suitable tailoring of the alloy composition (varying composition, doping, isostructural substitution, etc) it is possible to bring the two transitions together so that magnetic and structural transitions become coupled. Under these circumstances the alloy exhibits a single magneto-structural transition with giant magnetocaloric properties[85]. At this magneto-structural transition there is a large decrease in the volume of the unit cell ($\Delta v/v \sim 4$ %), and the transition temperature becomes extremely sensitive to the application of hydrostatic pressure ($dT/dp \simeq$ - 0.080 KMPa^{-1}).

Barocaloric studies were performed on a $MnCoGe_{0.99}In_{0.01}$ compound[86]. The experimental technique used in these studies was a simplified version of the quasi-direct method (improper quasi-direct). Differential scanning calorimetry measurements were conducted at atmospheric pressure and the $S(T)$ curves were obtained by combining these measurements with specific heat data. By assuming that the shape of $S(T)$ curves was not affected by hydrostatic pressure, they were shifted according to the pressure dependence of the transition temperature obtained from neutron experiments under pressure, in order to obtain successive $S(T,p)$ curves and to derive the isothermal entropy changes as detailed in section IV. Soon after, proper quasi-direct methods were used to investigate the barocaloric effect in $(MnNiSi)_{1-x}(FeCoGe)_x$ (x=0.38)[87].

The magneto-structural transition involves quite a large entropy change ($\Delta S_t \sim$ 55-65 Jkg^{-1}K^{-1}) which has been found to increase with increasing pressure ($d\Delta S_t/dp \simeq$ 0.040 Jkg^{-1}K^{-1}MPa^{-1}). The combination of a large entropy change and strong sensitivity of the transition temperature to pressure confers this type of alloys outstanding large inverse barocaloric properties. The associated entropy changes at pressures of $\sim$ 300 MPa are in the range $\Delta S^{qd} \sim$ 50-74 Jkg^{-1}K^{-1}, and directly measured temperature values of $\Delta T^d \sim$ 3-8 K. These temperature values are still much lower than those derived from $S(T,p)$ curves

$\Delta T^{qd} \sim$ 16-19 K, and values estimated from the entropy change ($\Delta T^{e} \sim$ 33-36 K).

Magnetic shape-memory alloys (MSMA) are the most widely studied family of magneto-structural materials for caloric and multi-caloric purposes. They share a lot of characteristics with the non-magnetic shape-memory alloys discussed in the previous section with the peculiarity that in MSMA the martensitic transition takes place in a magnetic state in such a way that the structural change is accompanied by changes in the magnetism of the material. The high temperature phase of MSMA is cubic, and orders ferromagnetically at the Curie temperature T_c^A, and the martensitic transition in these alloys can take place either above or below T_c^A. The technologically relevant properties arising from the coupling between structure and magnetism (magnetic shape memory, giant magnetocaloric effect, etc.) are enhanced in those alloys for which the martensitic transition takes place close or below T_c^A.

The martensitic transition in Fe-based magnetic alloys was studied many decades ago and some of these alloys, such as ordered Fe-Pt and Fe-Pd were shown to exhibit shape-memory properties[88]. These alloys order ferromagnetically, with a high Curie temperature ($T_c^A \sim$ 600-700 K), and at lower temperature they transform martensitically from a cubic $Fm3m$ towards a face-centered tetragonal martensite ($P4/mmm$). In Fe-Pd, this transition is weakly first-order, with a low entropy change ($\Delta S_t \simeq 1.2$ Jkg^{-1}K^{-1}), and low hysteresis[90]. There is no noticeable change in the volume of the unit cell and therefore no barocaloric effects are expected for this compound. The elastocaloric effect was studied in a $Fe_{68.8}Pd_{31.2}$ single crystal subjected to compressive uniaxial stresses along the [001] direction[89,90]. The transition temperature was found to increase very rapidly with increasing stress ($dT/d\sigma \simeq$ 1 KMPa^{-1}) as a consequence of the low ΔS_t value and a moderate shear strain at the transition. However, such an increase is limited to low stress values because of the existence of a critical point at $\sigma_c \simeq$ 40 MPa and $T_c \simeq$ 280K [91]. The entropy values obtained from strain vs. temperature curves at constant applied load are relatively small ($\Delta S^{i} \sim$ 4-5 Jkg^{-1}K^{-1}), but they are surprisingly larger than the transition entropy change ΔS_t. The fact that in this alloy the elastocaloric entropy change is not bounded by the transition entropy change is due to extreme softness of the lattice towards shear distortions (low value of the elastic constant C') which results in a marked temperature dependence of the associated shear strain even beyond the phase transition region, thereby leading to large values for the derivative $(\partial\varepsilon/\partial T)_{\sigma}$ which contribute to the isothermal entropy change (see equation 15) in addition to the latent heat of the transition (similarly to what occurs near a second-order

magnetic transition in magnetocaloric materials). Direct measurements of the adiabatic temperature change for stresses of 200 MPa give $\Delta T^d \simeq 3$ K. It is worth emphasizing that the low hysteresis of the transition together with strong sensitivity to the applied stress result in very good reproducibility of the elastocaloric effect upon stress cycling[92]. Furthermore, the elastocaloric effect has been found to span over a considerable temperature range (around 50 K).

With the exception of a few Fe-based alloys, the majority of MSMA belong to the family of Heusler alloys. These are Ni-based (and a few Co-based) Heusler alloys exhibiting an ordered cubic structure at high temperatures ($Fm3m$) which transforms martensitically towards a lower symmetry closer packed phase[93]. The mechanism of the martensitic transition is similar to that of non-magnetic alloys, and the particular structure of the martensitic phase depends on composition. Many different martensitic structures have been reported so far including non-modulated tetragonal martensite ($L1_0$), and modulated monoclinic ($5M$, $7M$, etc) and orthorhombic ($4O$) phases. Actually a detailed description of the several martensitic structures is still a subject of intense research and debate. It has been suggested that modulated structures can be described as an adaptive phase composed of nano-twinned tetragonal martensite variants[94], but there are experimental observations which do not support such a hypothesis[95]. For the mechanocaloric properties of MSMA, detailed knowledge of the actual crystallographic phase is not essential and therefore we will skip providing details of the space group of each investigated martensitic alloy. For present purposes it is enough to consider that all martensitic phases (tetragonal, orthorhombic and monocilinic) mostly involve a shear of the $\{110\}$ planes along the $< 1\bar{1}0 >$ directions of the cubic phase. As will be discussed below, in some of the alloys, the coupling between magnetism and structure can also give rise to a small volume change of the unit cell at the martensitic transition.

MSMA can be broadly classed into two categories depending on the magnetic properties of the martensitic phase. The first class includes alloys where the martensitic phase is ferromagnetic. In this case the change in magnetization at the martensitic transition is rather small (except for those alloys with concurrent Curie and martensitic transition temperatures) and the magneto-mechanical and magneto-thermal properties are mostly determined by the differences in magnetic anisotropy between cubic and martensitic phases[26]. The second class comprises those alloys for which the magnetic order below the martensitic transition is not ferromagnetic, and the magnetization of the martensitic phase is much lower than that of the

cubic phase. These alloys are also known as metamagnetic alloys, and the strong sensitivity of the transition to the magnetic field which is associated with the change in magnetization is at the origin of a number of relevant properties such as magnetic superelasticity[96,97] and inverse magnetocaloric effect[25] in these alloys. Actually, the magnetic state of the martensitic phase in metamagnetic shape-memory alloys is still under debate[98,99], but there is general agreement that antiferromagnetic correlations play a relevant role[100]. For many of the magnetic shape-memory alloys the volume change at the phase transition is rather small, but for a number of metamagnetic alloys, the interplay between magnetic and structural degrees of freedom results in a martensitic unit cell larger than that of the Heusler phase ($\Delta v/v \sim$ 0.5-1 %) so that the martensitic transition is sensitive to hydrostatic pressure[101] and these alloys are prone to exhibit the giant barocaloric effect, as will be discussed in the following.

The transition entropy change in MSMA contains two major contributions: vibrational and magnetic. The leading contribution is the vibrational contribution[102], which, as occurs in non-magnetic SMA, has its origin in the low-energy TA_2 phonons of the cubic phase[103,104]. For those alloys transforming martensitically between two ferromagnetically ordered states, the magnetic contribution is small and plays a minor role. However, in metamagnetic shape-memory alloys, the martensitic phase has a magnetic entropy larger than that of the cubic phase. Therefore, the vibrational and magnetic degrees of freedom contribute in an opposite way to the transition entropy change and, eventually, they can compensate each other in such a way that the martensitic transition no longer takes place. A detailed discussion on the significance of each contribution to the relative stability of cubic and martensitic phases can be found in ref. [105].

In contrast to non magnetic SMA, which feature very good mechanical properties, MSMA are very brittle and measurement of mechanocaloric effects becomes challenging. The first studies of the elastocaloric effect in this family of alloys were performed in Ni-Mn-Ga alloys doped with Fe [106] and Co [107] to improve their ductility. Uniaxial compression experiments were conducted on polycrystalline samples, where the applied load was kept at low values to prevent damaging the samples. The transition temperature was found to increase with increasing stress $dT/d\sigma \simeq 0.16$ KMPa^{-1} , giving rise to a conventional elastocaloric effect. Isothermal entropy changes were computed from strain vs temperature curves recorded at fixed values of applied load, and the values obtained were moderate as a consequence of

the low values of the applied stress ($\Delta S^i \sim$ 3-6 Jkg^{-1}K^{-1} for $\sigma \sim 10$ MPa).

There have been a number of strategies to improve the mechanical properties of magnetic shape-memory alloys. For Ni-Fe-Ga polycrystalline alloys it was found that the precipitation of secondary phases by means of suitable heat treatment enhanced the mechanical stability of the alloy. In these dual-phase alloys uniaxial compression stresses ($\sigma \simeq 170$ MPa) were applied which rendered temperature changes of $\Delta T^d \simeq 4$ K [108]. Better elastocaloric properties were found for single crystalline Ni-Fe-Ga[53,109] and Ni-Fe-Co-Ga[110]. Compression experiments were performed along the [011], [001] and [420] directions[53,109] and the highest stress-sensitivity of the transition temperature was found for stresses along [001] ($dT/d\sigma \simeq 0.7$ KMPa^{-1}) while lower values were found for other directions ($dT/d\sigma \sim$ 0.25-0.3 KMPa^{-1}). Significantly large values of adiabatic temperature change ($\Delta T^d \simeq 8$ K) were measured at relatively low values of the applied stress ($\sigma \simeq 30$ MPa)[109]. Slighlty larger values ($\Delta T^d \simeq 10$ K) were obtained for the Co-doped sample but for higher stresses ($\sigma \simeq 300$ MPa)[110]. The good elastocaloric performance of this MSMA is associated with the remarkably large shear strain ($\varepsilon \sim 14\%$) that accompanies the martensitic transition in this alloy system.

Co-Ni-Al alloys have better mechanical properties than the other MSMA and one could expect good elastocaloric performance for these materials. However, the martensitic transition occurs with larger hysteresis and the measured adiabatic temperature changes in a single crystal compressed along the [115] direction were significantly lower ($\Delta T^d \simeq 3$ K)[53] than those in Ni_2FeGa single crystals at $\sigma \simeq 150$ MPa.

The elastocaloric effect has also been studied in metamagnetic shape memory alloys. For this family of alloys first experiments were conducted on Cu-doped Ni-Mn-Sn alloys[111]. Uniaxial compression was restricted to very low values of the applied stress ($\sigma \simeq 10$ MPa), and the entropy values computed from stress vs temperature curves were low ($\Delta S^i \simeq 2$ Jkg^{-1}K^{-1}) due to the fact that a very small fraction of the sample underwent the martensitic transition for these low stress values. Later experiments on a Ni-Mn-Sb-Co sample, which exhibited better mechanical properties, were able to be conducted for stresses up to $\sigma \simeq 100$ MPa, and the obtained entropy changes were considerably large ($\Delta S^i \simeq 20$ Jkg^{-1}K^{-1}), but still lower than the total transition entropy change ($\Delta S_t \simeq 34$ Jkg^{-1}K^{-1})[112]. Significantly higher stresses ($\sigma \simeq 300$ MPa) were applied to a Co-doped Ni-Mn-Sn but the obtained entropy values ($\Delta S \simeq 12$ Jkg^{-1}K^{-1}) were lower than in Ni-Mn-Sb-Co due to a lower transition entropy change ($\Delta S_t \simeq 14$ Jkg^{-1}K^{-1}) of this compound[113]. With regards to the adiabiatic

temperature changes, direct measurements were reported for Ni-Mn-Sn which rendered values $\Delta T^d \simeq 6$ K for stresses of $\sigma \simeq 300$ MPa. These values are still significantly lower than the maximum values that could be obtained from the transition entropy change in these alloys[114].

One of the most important metamagnetic alloys is Ni-Mn-In and the quaternary Co-doped Ni-Mn-In-Co. For this alloy system, there is strong sensitivity of the transition temperature to magnetic field and the alloy is the prototype material exhibiting magnetic superelasticity[96,97]. Recently the alloy has also been shown to exhibit interesting mechanocaloric properties. Ni-Mn-In-Co textured polycrystals were uniaxially compressed along the [001] direction up to $\sigma \simeq 100$ MPa, with a resulting adiabatic temperature change of $\Delta T^d \simeq 4$ K [115]. Similar results were found for non-textured polycrystalline samples where it was shown that these ΔT^d values corresponding to the elastocaloric effect were reproducible upon cycling the sample for at least 15 cycles[116]. Textured polycrystalline Ni-Mn-In was also investigated for stresses up to $\sigma \simeq 250$ MPa, and the obtained values ($\Delta T^d \simeq 4$ K) were similar to those of the Co-doped compounds[117]. In all these cases it should be pointed out that these relatively low values correspond to a partial transformation of the sample.

As previously mentioned, those MSMA with a significant change in the magnetic properties accross the martensitic transition (many metamagnetic shape-memory alloys) may exhibit a relatively large change in the volume of the unit cell. In the important class of NiMn-based MSMA this can be explained taking into account the fact that magnetic moments are localized at Mn-atoms to a very good approximation and are coupled through an oscillatory RKKY-type exchange interaction mediated by conduction electrons. This explains the fact that magnetic properties in this class of materials are extremely sensitive to small changes in the distances between Mn-atoms[118]. In Mn-rich non-stoichimetric alloys that undergo a martenitic transition, this effect leads to strong competition between ferro- and antiferromagnetism, which arises from the existence of nearest-neighbor Mn-pairs[119]. The volume reduction taking place at the transition enables the stability of the martensitic phase to be enhanced and thus reflects the strong sensitivity of the the magnetic interactions to the distance between localized magnetic moments. In these alloys, the martensitic transition temperature significantly increases with the application of hydrostatic pressure[101] and they are prone to exhibit barocaloric effects.

Although some preliminary studies of barocaloric effects were conducted for some rare-earth materials, they did not receive to much attention because the effects were too small[120]. Actually, the Ni-Mn-In magnetic shape-memory alloy was the first compound reported to exhibit a giant barocaloric effect[121]. Calorimetric experiments under hydrostatic pressure were performed on a $Ni_{49.26}Mn_{36.08}In_{14.66}$ polycrystal. The martensitic transition temperature was found to increase with pressure ($dT/dp \simeq 0.018$ KMPa^{-1}), in agreement with pressure stabilizing the lower volume martensitic phase. The associated barocaloric effect was conventional, with relatively large values for the isothermal entropy change ($\Delta S^{qd} \simeq 24$ Jkg^{-1}K^{-1}) for $p \simeq 250$ MPa. This value is only slightly lower than the transition entropy change $\Delta S_t \simeq 27$ Jkg^{-1}K^{-1} in this compound.

A later systematic study was conducted on Ni-Mn-In samples with tailored compositions for which the martensitic transition exhibited very narrow hysteresis (around 5 K), and with transition temperatures covering a broad range[122]. It was found that samples transforming martensitically close to and above the Curie point exhibited the largest values for the entropy change ($\Delta S^{qd} \simeq 35$ Jkg^{-1}K^{-1} at $p \simeq 250$ MPa). These large values were associated with large values of the transition entropy change. Indeed ΔS^{qd} was found to depend upon the relative distance between T_t and T_c^A, exhibiting behavior which parallels that of ΔS_t. Hence, as the martensitic transition approaches the Curie point, the magnetic contribution to the entropy change decreases, which results in an increase of ΔS_t (it is worth remembering that magnetic and vibrational contributions have opposite signs in metamagnetic SMA). The adiabatic temperature changes computed from these calorimetric measurements were in the range $\Delta T^{qd} \simeq$ 3-4 K. These lower values are due to the small shift of the transition with pressure which also results in poor reproducibility of the barocaloric effect in metamagnetic SMA.

The pressure sensitivity of the martensitic transition was enhanced in metamagnetic alloys with tailored compositions with a relatively large volume change at the martensitic transition[123]. Barocaloric experiments were conducted on $Ni_{42.7}Co_{8.87}Mn_{31.67}Ga_{14.98}In_{2.01}$, with a relative volume change at the transition $\Delta v/v \sim 0.7$ %. The shift in the transition temperature with pressure $dT/dp \simeq 0.030$ KMPa^{-1} was larger than for Ni-Mn-In compounds ($dT/dp \simeq 0.020$ KMPa^{-1}) but the values obtained for the entropy change ($\Delta S^{qd} \simeq 16$ Jkg^{-1}K^{-1} at $p \simeq 250$ MPa) were lower due to a much lower value of the transition entropy change ($\Delta S_t \simeq 21$ Jkg^{-1}K^{-1})[124].

A comparison of elastocaloric and barocaloric effects in metamagnetic shape-memory alloys shows that although the shift with pressure is smaller than with a uniaxial load, the final barocaloric ΔS values are slightly larger than for the elastocaloric case because hydrostatic pressure is not compromised by the intrinsic brittleness of the material and larger pressures can be applied. Nevertheless, the stronger sensitivity of the transition temperature to uniaxial stress ensures good reproducibility for the elastocaloric effect while poor reproducibility is found in the barocaloric effect.

VIII. MATERIALS WITH ELECTRO-STRUCTURAL TRANSITIONS

Materials undergoing polar phase transitions are considered promising candidates for electrocaloric refrigeration[15]. Many of these materials show a strong coupling between polar and structural degrees of freedom and changes in the unit cell can also take place at the ferroic transition. As a result, the transition turns out to be sensitive to applied external stresses and mechanocaloric effects are expected to occur in these materials.

The textbook ferroelectric material is $BaTiO_3$. At high temperature it has a cubic perovskite structure ($Pm\bar{3}m$), which upon cooling, transforms towards a tetragonal ($P4mm$) phase at a temperature $T_t \simeq 400$ K. The tetragonal unit cell has a volume slightly larger than the cubic cell ($\Delta v/v \sim 0.11$ %) and results from the expansion of one of the cube edges to form the tetragonal c axis and a compressioon of the two other edges to form the tetragonal a axes. This distortion causes a relative displacement between titanium and oxygen atoms that gives rise to spontaneous polarization along the tetragonal c axis. Upon further cooling, the tetragonal phase transforms towards an orthorhombic phase ($Bmm2$) at $T_t \simeq 270$ K. The orthorhombic phase is still ferroelectric but the spontaneous polarizaton is parallel to the original cubic $< 110 >$ direction. At even lower temperatures the orthorhombic phase transforms towards a rhombohedral phase ($T_t \simeq 180$ K), with a polar axis lying along one of the original $< 111 >$ directions[125]. There was some controversy on whether the volume of the orthorhombic phase was larger or smaller than that of the tetragonal phase, but it is now established that the orthorhombic phase has a slightly larger volume ($\Delta v/v \sim 0.03$ %). These phase transitions have a relatively low latent heat, with transition entropy changes $\Delta S_t \simeq 2.4$ Jkg^{-1}K^{-1} for the cubic-tetragonal transition and $\Delta S_t \simeq 2$ Jkg^{-1}K^{-1} for the tetragonal-orthorhombic phase. The major contribution to ΔS_t comes from the polar

degrees of freedom. The characteristics of the transition are well reproduced by a Landau model with polarization as the order parameter[126]. With regards to the orthorhombic-rhombohedral transition, both the volume change and entropy change of the compound are very small ($\Delta S \simeq 0.5$ Jkg^{-1}K^{-1}) and this transition has not received so much attention.

Calorimetric measurements under hydrostatic pressure were performed on $BaTiO_3$ ceramics, over a temperature range covering both cubic-tetragonal and tetragonal-orthorhombic transitions[127]. Both transition temperatures were found to decrease with increasing pressure: $dT/dp \simeq$ -0.055 KMPa^{-1} for the cubic-tetragonal and $dT/dp \simeq$ -0.03 KMPa^{-1} for the tetragonal-orthorhomic in agreement with pressure stabilizing the high temperature high-volume phases. Accordingly, the barocaloric effect associated with both transitions was found to be inverse. The transition entropy change was found to slightly decrease with increasing pressure due to contributions beyond the phase transition. The isothermal entropy change associated with the barocaloric effect was found to be maximum for an applied pressure of $p \simeq 100$ MPa with values $\Delta S^{qd} \simeq 1.7$ Jkg^{-1}K^{-1} for the cubic-tetragonal transition and $\Delta S^{qd} \simeq 1.2$ Jkg^{-1}K^{-1} for the tetragonal-orthorhombic transition. Further pressure increases resulted in a decrease of the entropy change due to the decrease of ΔS_t with pressure. A salient feature in $BaTiO_3$ is that the entropy values associated with the barocaloric effect at the cubic-tetragonal transition are expected to be reversible upon pressure cycling in a temperature range of ~ 15 K.

Another ferroelectric ceramic with barocaloric effects is $PbTiO_3$ [128]. This compound also exhibits a cubic ($Pm\bar{3}m$) - tetragonal ($P4mm$) transition but at a much higher temperature ($T_t \simeq 700$ K) than $BaTiO_3$. In the high temperature cubic phase Pb atoms are disordered and, with an equal probability, occupy one of the six positions associated with the displacement of the atoms from the (0,0,0) position by a certain amount in the $< 001 >$ directions. In the low temperature phase a partial ordering of Pb atoms in one of the positions occurs. The entropy change at the cubic-tetragonal transition is associated with such an order-disorder process and it amounts to $\Delta S_t \simeq 27$ Jkg^{-1}K^{-1}. The barocaloric effect in this compound was investigated by performing calorimetric measurements at atmospheric pressure and shifting the calorimetric curves according to the pressure dependence of the transition temperature obtained from other techniques (improper quasi-direct method). The tetragonal unit cell has a volume larger than the cubic cell ($\Delta v/v \sim 0.4$ %), and the transition temperature decreases with increasing pressure. There is a large scatter in the data

for dT/dp reported in the literature, and the value used to compute barocaloric effects was obtained from thermal expansion data to be $dT/dp \simeq$ -0.140 KMPa^{-1}. The isothermal entropy and adiabatic temperature values obtained at pressures of $p \simeq 260$ MPa were quite moderate $\Delta S^{qd} \simeq 2.7$ Jkg^{-1}K^{-1} and $\Delta T^{qd} \simeq 1.9$ K.

Inorganic salts represent a very interesting family of compounds. Among them ammonium sulphate and a number of fluoride salts have been shown to present outstanding barocaloric properties.

Ammonium sulphate [$(NH_4)_2O_4$] adopts a centrosymmetric orthorhombic structure ($Pnam$) with four formula units per unit cell comprising three ionic groups. On cooling, the material undergoes an electro-structural transition at $T_t \simeq 220$ K towards a polar orthorhombic structure ($Pna2_1$) that is ferrielectric. In the high temperature phase, the ionic groups adopt a disordered configuration, and they become ordered below T_t giving rise to a ferrielectric phase[129,130]. The ordering of these ionic groups occurs in two steps: firstly there is a first-order phase transition at T_t causing partial ionic ordering, and secondly additional ordering takes place continuously on cooling down to $\simeq 160$ K. The entropy difference between the $Pnam$ and $Pna2_1$ phases is due to the order-disorder of these ionic groups and amounts to $\Delta S_t \simeq 130$ Jkg^{-1}K^{-1}, whereas the entropy change at the first-order phase transition ($\Delta S_t \simeq 65$ Jkg^{-1}K^{-1}) associated with partial ordering of the ionic groups is about half of the total transition entropy change. The order-disorder transition also involves changes in the volume of the unit cell, where the unit cell of the fully ordered orthorhombic phase is about 1 % larger than that of the disordered phase ($\Delta v/v \sim 1$ %). At the first-order phase transition the relative volume change is $\Delta v/v \sim 0.5$ %.

Calorimetry under hydrostatic pressure was conducted in an ammonium sulphate powder near the ferrielectric phase transition[131]. The transition temperature was found to significantly decrease when applying pressure ($dT/dp \simeq$ -0.050 KMPa^{-1}), in agreement with the higher volume of the low temperature phase. Accordingly the barocaloric effect in this material is inverse. Significantly large values for the isothermal entropy ($\Delta S^{qd} \simeq 60$ Jkg^{-1}K^{-1}) were obtained at a low pressure of $p \simeq 100$ MPa. Within experimental error, these values were coincident with the entropy change corresponding to the first-order phase transition and indicated that in this compound low pressure was enough to drive the whole material through the first-order phase transition. Another interesting peculiarity of the ferrielectric transition in ammonium sulphate is that the strong sensitivity of the transition to pressure

added to very weak thermal hysteresis confer a very good reproducibility of the barocaloric effect upon cycling pressure over a temperature range of ~ 10 K.

While differential scanning calorimetry is very well suited to measuring entropy changes at first-order phase transitions, this technique is not adequate to determine contributions to the entropy change due to continuous change in volume with temperature beyond the phase transition. These contributions are negligible for most mechanocaloric materials (with thermal expansion coefficients in the range 10^{-5}-10^{-7} K^{-1}) but they are relevant in ammonium sulphate with a significantly larger thermal expansion coefficient (10^{-4} K^{-1}). These contributions can be estimated by the indirect method (equation 4) from volume vs temperature curves. It was found that in ammonium sulphate these contributions were responsible for the decrease in the measured isothermal entropy change as pressure was increased.

Fluoride salts have attracted interest because the existence of polar noncentrosymmetric structures (typically fluorine-oxigen octahedra and ammonia tetrahedra) should make possible various polar structures with important properties including ferroelectrictity and piezo-electricity. However, these salts crystallize in a variety of structures and most of them are centrosymmetric due to a statistical orientational disorder of the inherent polar groups[132]. Upon cooling many of these salts undergo a structural transition towards a lower symmetry phase where the disordered polar structures become totally or partially ordered with the associated decrease in configurational entropy. Such an entropy change depends on the particular crystal symmetry of the high and low temperature phases and for specific structures it can reach significantly large values up to $R \ln 12$ associated with the possible orientational configurations of polar groups. In most fluoride salts there is no development of a spontaneous polarization and the transitions are classed to be non-ferroelectric.

For a number of fluoride salts, there is a difference in the unit cell volume of the high and low temperature phases and the phase transition is sensitive to applied pressure. Such strong sensitivity along with the large transition entropy change of the phase transition make fluoride salts excellent candidates for barocaloric effects. Several studies of barocaloric properties have been reported for a variety of fluoride salts[133–136]. Experiments were conducted by DSC runs at atmospheric pressure to determine the entropy curves, and shifting these curves with pressure according to the pressure dependence of the transition temperature determined by other experimental technique (improper quasi-direct method). Most of the studied compounds included the ammonia group $(NH_4)^+$ and the structural transition

involved ordering of both ammonia tetrahedra and fluorine-oxigen octahedra.

The metallic atom in the $(NH_4)_2ZO_2F_4$ (Z= W, Mo) and $(NH_4)_2NbOF_5$ salts was found to play a relevant role in the crystallographic structure adopted by the compounds and thereby in their barocaloric properties. In the Nb salt, barocaloric effects were associated with the occurrence of two consecutive structural transitions with a significantly large overall entropy change ($\Delta S_t \simeq 155$ Jkg^{-1}K^{-1})[133] while in the other two compounds it was due to a single transition[134]. Hydrostatic pressure was found to stabilize the high temperature phase in the Nb compound ($dT/dp \simeq$ -0.045 KMPa^{-1}) while it stabilized the low temperature phase in the W ($dT/dp \simeq 0.093$ KMPa^{-1}) and Mo ($dT/dp \simeq 0.013$ KMPa^{-1}) compounds. The computed isothermal entropy change for the inverse barocaloric effect in the the Nb compound was remarkably large ($\Delta S^{qd} \simeq 100$ Jkg^{-1}K^{-1}) as a result of the large transition entropy change. However, the obtained value was still lower than the transition entropy change, indicating a partial transformation of the sample for quite large applied pressures ($p \simeq 1000$ MPa).

Oxygen-free $(NH_4)_2SnF_6$ was also shown to exhibit relatively large barocaloric properties[135]. This compound features very large sensitivity of the transition temperature with pressure ($dT/dp \simeq$ -0.157 KMPa^{-1}) which gives rise to a large inverse barocaloric effect ($\Delta S^{qd} \simeq$ 61 Jkg^{-1}K^{-1}) at low applied pressure ($p \simeq 100$ MPa). Finally, barocaloric effects were also reported for fluorine salts where ammonia ions are replaced by alkali metals[136]. The isothermal entropy change obtained for Rb_2KTiOF_5 at $p \simeq 600$ MPa compares well ($\Delta S^{qd} \simeq$ 46 Jkg^{-1}K^{-1}) to those found for the rest of fluorine salts.

When comparing barocaloric data between magneto-structural and electro-structural materials attention has to be paid to the differences in density between the two classes of compounds. In general, the reported values for the isothermal entropy change for the barocaloric effect in inorganic salts are larger than those obtained in magnetic metallic alloys. However, it is to be noticed the fact that inorganic salts feature much lower densities than metallic alloys, and therefore the volumetric values for the entropy changes are comparable for the two families of compounds. Actually, in spite of the larger mass entropy change, the reported values for the adiabatic temperature change are comparable owing also to a larger mass specific heat in the inorganic salts.

With regards to the elastocaloric effect in polar materials, a few theoretical approaches have been made using first principle calculations[137–139] and phenomenological models[140,141] in

ferroelectric $BaTiO_3$, $Ba_{0.5}Sr_{0.5}TiO_3$ and $PbTiO_3$. Unbounded large values for the adiabatic temperature change are predicted for stresses in the order of GPa, but for more experimentally available stresses ($\sigma \simeq 200$ MPa) the predicted values are in the range 3-6 K. From the experimental side, attempts have been made[142–144] to analyze previously published data on the behavior of $Pb(Mn_{1/3}Nb_{2/3})O_3$-32$PbTiO_3$ single crystals, $(Ba_{0.85}Ca_{0.15})(Zr_{0.1}Ti_{0.0})O_3$ and PZT ceramics under stress. Data computed for the adiabatic temperature change are low $\Delta T^i \sim 0.2$ - 2 K, and in many cases they do not exhibit a monotonic dependence upon applied stress. Experiments particularly designed to provide reliable values for the adiabatic temperature and isothermal entropy changes seem to be necessary to gain full characterization of elastocaloric effects in polar materials undergoing electro-structural transitions.

IX. COMPARISON OF ELASTOCALORIC AND BAROCALORIC MATERIALS

In the preceding sections we have reviewed the mechanocaloric properties of materials based on the physical properties at their structural phase transitions. In this section we provide a (graphical) comparative view of these materials in terms of their caloric effects: elastocaloric and barocaloric.

Figures 2 and 3 illustrate, respectively, the shift in the transition temperature with uniaxial stress and hydrostatic pressure. The inset in Figure 2 shows an enlarged view for the low stress region. Lines have been plotted according to the slopes listed in Tables 1 and 2, and the length of these lines is indicative of the maximum applied stress in the study of each particular compound. A first salient feature in comparing the two figures is that, in general, uniaxial stress is more effective in shifting the transition than hydrostatic pressure. Such strong sensitivity will be beneficial for the reproducibility of the elastocaloric effect and for achieving a very broad temperature interval of applicability of the elastocaloric effect.

With regards to elastocaloric materials (Fig. 2), magnetic shape-memory alloys (MSMA) have $dT/d\sigma$ values in the range of those for Ni-Ti alloys, except for Ni-Fe-Ga, which has a large transitional shear strain. However, the range of stresses applicable to brittle MSMA is lower than for the more ductile non magnetic SMA. Among these conventional SMA, in Cu-based alloys the shift in transition temperature with stress is very large. It is also worth mentioning the case of Fe-Pd. Although the martensitic transition is extremely sensitive to uniaxial stress, the first-order character of the transition weakens as stress is increased

until a critical point is reached for stresses $\sigma \simeq 40$ MPa. The good ductility of the alloy supports application of stresses much larger than this value but with low elastocaloric entropy and temperature values. Finally, it must be noted that Fe-Rh alloys feature a very weak dependence of the transition with uniaxial stress which reflects the fact that the lattice distortion at the magneto-structural transition is a pure dilation. This also explains the decrease in transition temperature with increasing uniaxial tensile stress. In contrast, under uniaxial compressive stress the transition temperature increases with increasing stress at a rate similar to the tensile case but with opposite sign[145].

In barocaloric materials (Fig. 3) the transition temperature increases with pressure for those compounds with a lower volume, low temperature phase and decreases for those compounds with the low-temperature phase with a larger volume. The latter will display an inverse barocaloric effect: the material will exhibit the abnormal behavior of increasing the entropy when pressure is applied isothermally and cooling down when it is applied adiabatically. The inverse nature of the barocaloric effect is due to a coupling between structural and other degrees of freedom (magnetic and polar). The compounds with the highest shift in transition temperature with pressure are ionic salts which are less compact than magnetic and ceramic counterparts. On the other hand, although $PbTiO_3$ also seems to exhibit strong dependence, it must be taken into account that reported dT/dp data in the literature are very sparse and the value plotted in Fig. 3 corresponds to the highest reported value. Finally, it should be pointed out that the martensitic transition in metamagnetic SMA displays weak pressure sensitivity because the lattice distortion for this transition is mostly accomplished by a shear mechanism, accompanied by a small volume change.

In Figures 4 and 5 we have plotted the uniaxial stress and pressure dependencies of the isothermal entropy change (in absolute values) for selected elastocaloric and barocaloric compounds, respectively. The inset in Figure 5 shows the expanded view up to large values of applied pressure.

For elastocaloric materials (Fig. 4), the $B2 \leftrightarrow B19'$ has the largest entropy values, but owing to the considerable hysteresis of this transition, it is not expected that they are reproducible at low stress-values, and large stresses are required to achieve reproducibility. Interestingly, Cu-based alloys reach the maximum entropy value (which coincides with the transition entropy change) at very low values of applied stress. This results in very good reproducibility of the elastocaloric effect which makes these alloys excellent candidates for

low stress applications. The elastocaloric properties of Fe-Rh are weak, as expected from the fact that the structural change at the transition is a pure dilation.

In barocaloric materials (Fig. 5), ionic salts exhibit the largest values for the isothermal entropy change. However, it must be taken into account that the density of these compounds is three to four times lower than that of polar ceramics and magnetic alloys (see Table 2). This difference results in volumetric values for the entropy change in the range of those for magnetic compounds, and also the corresponding adiabatic temperature values are in the same range or even slightly lower. Among magneto-structural barocaloric compounds, those based on MnNiSi exhibit the largest entropy values (associated with a large transition entropy change and strong sensitivity of the transition to hydrostatic pressure). The barocaloric properties of ferroelectric ceramics is quite limited.

Finally, in Figures 6 and 7 we have plotted adiabatic temperature changes as a function of the isothermal entropy. We have used different symbols to indicate the different experimental techniques used to derive these temperature values (see section IV for details). We have also included the expected temperature change in the figure (open circles) that would correspond to the adiabatic release (or absortion) of the latent heat of the transition. For most of the materials this value represents the upper limit for the adiabatic temperature change that can be obtained in the elastocaloric and barocaloric effect. It is obvious from the two figures that different experimental techniques can yield very disparate results, which highlights the fact that comparison between different materials (and different caloric effects) has to be done very cautiously, paying special attention on how the different data (entropy and temperature) have been determined.

For elastocaloric materials (Fig. 6), direct measurements (plotted as stars) coincide (in many cases) with the maximum estimated value (open circles) which indicates that direct techniques provide reliable values, and the applied stress was large enough to drive the whole sample through the structural transition. Remarkably high temperature and entropy values have been found for the $B2 \leftrightarrow B19'$ transition in Ni-Ti. These values are much larger than those reported for any other caloric effect, and evidence the enormous potential of elastocaloric cooling technologies.

For barocaloric materials (fig. 7) directly measured values for the adiabatic temperature change (stars) are much smaller than data derived from other techniques. This discrepancy is due to the lack of adiabaticity associated with the pressure transmitting fluid in the direct

measurements under hydrostatic pressure. According to the transition entropy changes, the maximum values that could be obtained in barocaloric experiments are in the range of $\sim$ 40 K, but they have not been reached yet, mostly due to the fact that within the studied pressure range, only partial transformation of the sample was achieved. It is worth noticing that for samples that were fully driven through the transiton (such as Fe-Rh and a few inorganic salts) there is good coincidence between the maximum temperature values (circles) and data derived from quasi-direct methods (triangles).

X. OTHER MATERIALS

Mechanocaloric effects have also been reported for a limited number of non-crystalline materials which are discussed in this section.

As mentioned in the introduction, natural rubber was the first reported material to exhibit elastocaloric effects[2]. Since that early report the effect did not receive major attention, but with the increasing interest in mechanocaloric materials, the caloric properties of natural rubber have recently been revisited[146–149]. In its natural state, rubber is an elastomer composed of polymeric chains which are randomly oriented. Applying stress to natural rubber causes orientation of polymeric chains along the stress direction thereby leading to an increase of configurational order with the associated decrease in entropy. In natural rubber there is strain-induced crystallization with a latent heat that contributes significantly to its giant elastocaloric effect. Tensile experiments were conducted on natural rubber for temperatures around room temperature. Experiments conducted at low strain rates enabled the indirect determination of isothermal entropy and adiabatic temperature changes. Indirect temperature data were compared to direct measurements made by thermocouples and thermal imaging at much faster strain rates (adiabatic limit). The computation of temperature changes from experiments of strain vs temperature at constant stress yielded values that did not match to directly measured values. However, measuring stress vs temperature at constant strain resulted in ΔT^i values close to the directly measured ones ($\Delta T^d \sim$ 9-12 K for a strain of $\varepsilon \sim 600$ %, with a corresponding stress of $\sigma \sim$ 1-2 MPa)[148,150]. The entropy change was found to linearly increase with sample elongation, with a maximum value estimated from the measured temperature change of $\Delta S^e \simeq 80$ Jkg^{-1}K^{-1} (for $\varepsilon \simeq 600$ %, $\sigma \simeq$ 1-2 MPa).

An interesting family of caloric materials are the polymers based on PVDF (polyvinylidene fluoride). These polymers can exist in five different crystalline forms. Copolymers and terpolymers are particularly relevant because they have been shown to exhibit excellent electrocaloric properties associated with their ferroelectric properties[151]. In these polymers, the polar β phase is stable below the Curie point and it has been shown that mechanical stresses modify the relative stability between this phase and the anti-polar α phase. The β unit cell has a 2.5 % smaller volume than the α phase and therefore hydrostatic pressure shifts the α-β transition towards higher temperatures.

The pressure dependence of the α-β transition was investigated for a copolymer (65% VDF and 35% TrFE) and a terpolymer (61.1 % VDF, 32.2 % TrFE and 6.2 % CTFE) by isobaric and isothermal volume measurements at hydrostatic pressures up to 200 MPa [152]. A moderate shift in the transition temperature was found for the coploymer but in the terpolymer the transition temperature significantly increased with increasing pressure ($dp/dT \simeq 0.250$ KMPa^{-1}). The data for the terpolymer were later analysed[153] to compute the barocaloric effect. A significantly large isothermal entropy change ($\Delta S^i \simeq 120$ Jkg^{-1}K^{-1}) was found for $p \simeq 200$ MPa, which is slightly lower than the transition entropy change $\Delta S_t \simeq 150$ Jkg^{-1}K^{-1}. The adiabatic temperature change was also estimated using eq. 8. However in ref. [153] the calorimetric data used to derive C were taken from DSC curves (which do not provide reliable data for specific heat) that corresponded to the copolymer. By means of modulated calorimetry, properly measured data for C in copolymers and terpolymers of similar composition were reported in [151]. By using these values, the estimated adiabatic temperature change for therpolymers is $\Delta T^e \simeq 28$ K for $\sigma \simeq 200$ MPa.

Relaxor polymers have also been shown to exhibit interesting elastocaloric properties[154]. Direct measurements of the adiabatic temperature change by means of a thermal camera have been performed on P(VDF-TrFE-CTFE) terpolymers subjected to uniaxial tensile stresses. It has been found that ΔT^d monotonously increased with increasing the applied stress, and reached values $\Delta T^d \sim$ 2-3 K for maximum applied stresses of ~ 150 MPa. This maximum stress corresponded to a strain $\varepsilon \sim 12$ %, and for larger stresses non linear stress strain behaviour was obtained. The estimated isothermal entropy change corresponding to the maximum measured temperature change amounts to $\Delta S^e \simeq 21$ Jkg^{-1}K^{-1}.

Relevant mechanocaloric effects also occur in poly(methyl methacrylate), PMMA. Temperature changes resulting from rapid hydrostatic pressure variations were measured at

various temperatures from room temperature up to ~ 370 K in a range of pressures up to 200 MPa [155]. ΔT^d values were found to monotonously increase with increasing pressure, and they also increase with increasing measuring temperature. Such an increase is enhanced at temperatures close to the glass transition temperature ($T_g \simeq 370$ K). A considerably large value $\Delta T^d \simeq 9$ K was measured at $p \simeq 200$ MPa just below the glass transition temperature. Interestingly enough, ΔT^d values were found to be reproducible upon increasing and decreasing pressure for many cycles, displaying a good reversibility.

XI. MULTICALORIC EFFECTS

In the previous sections we have seen that many of the most studied magneto- and electrocaloric materials also show interesting mechanocaloric properties (either elasto- or/and barocaloric effects). Actually, in many magneto- and electrocaloric materials the first-order character of the transition at the origin of the large (or even giant) thermal response to applied magnetic or electric fields is a consequence of the strong interplay between lattice and magnetic or polar degrees of freedom. Therefore, due to a cross-response to mechanical and magnetic or electric fields, magneto- or electro- and mechanocaloric effects are expected to directly influence each other and thus, these materials should be classified as multicaloric materials[9]. However, so far relatively little research efforts have been devoted to the study of these combined magneto-mechanic or electro-mechanic thermal effects. At present, most of the reported results refer to the study of the effect of an applied hydrostatic pressure on magneto- and, to a much less extent, electrocaloric effects. In this section, we will compile the main results reported along these lines.

From the above-discussed perspective, the influence of pressure on prototype magnetocaloric materials such as MnAs, Gd-Si-Ge and La-Fe-Si has been reported. In these materials, the application of pressure produces quite diverse effects on the magnetocaloric response. In MnAs it has been found that their magnetocaloric effect is strongly enhanced by application of a moderate hydrostatic pressure[156]. The maximum entropy change induced from isothermal application of a magnetic field of 5 T has been reported to increase from 40 $\mathrm{Jkg^{-1}K^{-1}}$ at ambient pressure to 267 $\mathrm{Jkg^{-1}K^{-1}}$ for an applied moderate pressure of 223 MPa. This huge increase has been attributed by the authors to the contribution of the lattice degrees of freedom. However, since the obtained value largely overcomes the

transition entropy change, it could be affected by the spurious peak effect originated by an inappropriate measurement protocol[157,158].

The effect of hydrostatic pressure on the magnetostructural transition in $Gd_5(Si_xGe_{1-x})_4$ compounds has been reported in Ref. [159]. For high Ge content, the transition temperature increases with applied pressure with a moderate rate of $dT/dp \simeq 0.003$ KMPa^{-1}, while by increasing the content in Si, the rate strongly increases and close to the $Gd_5Si_2Ge_2$ stoichiometry it is one order of magnitude larger. This behavior suggests that applied pressure should significantly affect the magnetocaloric properties of this material in the Si-rich region of the phase diagram. For $Gd_5Si_2Ge_2$ the magnetocaloric effect was found to decreas with increasing pressure[160] since this makes the magnetostructural transition from the monoclinic to orthorhombic structures approach the Curie temperature of the monoclinic phase. At an applied pressure of 600 MPa both transitions merge into a single one, which becomes second order. Above this pressure, the magnetocaloric effect remains independent of pressure and displays the expected features associated with a second order transition.

In both La-Fe-Si and La-Fe-Si-hydrides the magnetostructural transition is shifted to lower temperatures by increasing the applied pressure[161]. However, while the magnetocaloric effect is found to weaken in $LaFe_{11.57}Si_{1.43}$ when hydrostatic pressure is applied, it is enhanced in the $LaFe_{11.57}Si_{1.43}H_{1.64}$ hydride. This opposite behavior of parent and hydrogenated compounds reflects the fact that while the magnetization change at the magnetostructural transition strongly decreases by application of pressure in La-Fe-Si, it remains almost pressure independent in the hydrides due to the interstitial loction of the H atoms. This result indicates that the effect of pressure on the magnetocaloric effect is very sensitive to specific features of the magnetostructural interplay.

Pressure experiments in hexagonal Ni_2In-type $Mn_{1-x}Cr_xCoGe$ compounds[162] reveal that pressure is able to tune the temperature at which the magnetostructural phase transition occurs. However, the magnitude of the magnetocaloric effect is almost insensitive to the applied pressure. In mixtures of $(MnNiSi)_{1-x}(MnFeGe)_x$ of similar Ni_2In-type hexagonal compounds it has been shown that fine tuning of the fraction of each component moves the magnetostructural transition close to room temperature and maximizes the volume change at the transition[163]. The designed material, obtained by alloying 46% of MnNiSi with 54% MnFeGe, displays a huge relative volume change of about 7% at the transition, which leads to a giant enhancement of the magnetocaloric effect under application of moderate pressures.

This material was later used to study barocaloric effects[87], as discussed in the previous sections.

Heusler shape-memory alloys have also been studied from this perspective. The effect of pressure on the magnetocaloric properties of the Heusler Ni-Co-Mn-Sb alloy has been reported in Ref. [164]. In this system the magnetocaloric effect is inverse and application of a magnetic field shifts the martensitic transition to lower temperatures, while application of hydrostatic pressure has an opposite effect. In these compounds application of pressure has little effect on the magnitude of magnetic field-induced entropy change but enables tuning of the magnetocaloric effect over a large temperature range about room temperature, which improves the potential refrigerant capacity of these systems. More recently, it has been shown that it is possible to also take advantage of this behavior in order to effectively decrease the hysteresis and improve the reproducibility of the caloric effect. In a Ni-Mn-In-(Co) Heusler alloy it has been shown that by magnetizing at atmospheric pressure and demagnetizing at an applied pressure, the effective hysteresis can be considerably reduced[165]. Indeed, a similar procedure can be applied to tune hysteresis in any caloric material that responds to two applied fields.

In the case of Heusler alloys, the influence of a magnetic field on the elastocaloric effect induced by the application of uniaxial compressive stress has been reported in Ref. [107]. In spite of the fact that only relatively low stresses (up to $\simeq$10 MPa) were applied due to poor mechanical properties of this class of materials, results show that the elastocaloric effect is significantly improved. Actually, application of a magnetic field below 1 T enables the elastocaloric relative cooling power (RCP) to be improved by about 20%. Similarly, the effect of an applied electric field on the elastocaloric response of ferroelectric $Pb(Mn_{1/3}Nb_{2/3})O_3$-$32PbTiO_3$ single crystals was estimated in [142]. However, in this case the effect has been found to be quite small.

Theoretical models have been proposed to account for multicaloric effects. In Ref. [166] the multicaloric properties of Heusler alloys have been reproduced by means of a Landau model that incorporates the adequate, symmetry allowed, interplay between magnetic and structural order parameters. The combination of the Landau approach with first principle calculations seems to be a good strategy to predict efficient mechanisms leading to an enhancement of the interplay between ferroic properties that could provide new routes for designing new materials with optimal caloric properties. Within this viewpoint, the study

of multicaloric effects in the ferroelectric-ferroelastic $PbTiO_3$ oxide, has predicted unusual adiabatic temperature changes induced by simultaneous application of stress and electric field, that are expected to significantly exceed the values associated with either elasto- or electrocaloric effects alone in the same material[167].

XII. DEMONSTRATORS AND PROTOTYPE DEVICES FOR COOLING

Although the study of mechanocaloric effects for solid-state refrigeration is still an incipient discipline, much less mature than for magnetocaloric and electrocaloric counterparts, a few prototypes and demonstrators have already been developed[168–173]. A thorough description of these prototypes falls beyond the scope of the present paper, but we provide below some key features of these devices. A more detailed description can be found in Ref. [174].

Until now there has not been any proposed prototype working under hydrostatic pressure, based on the barocaloric effect. In contrast, several elastocaloric prototypes have been developed. In all those prototypes the working element (refrigerant material) is a non-magnetic shape-memory alloy (most of the Ni-Ti based SMA), and the devices can be broadly classed into two major categories, depending on the method they use to transfer heat from the cool to the heat sinks/sources[174].

The first class refers to those devices where the SMA element is stationary, and a heat transfer fluid cyclically flows to transfer heat. With such a working principle, a prototype based on multiple Ni-Ti tubes was developed[168]. The tubes were compressed by a motor driven screw-jack. An interesting feature of this device is the possibility of recovering the unloading work when the SMA transforms from martensite to austenite. This is achieved by a symmetric layout and pre-compressing the tube beds. An improved design has recently been proposed[169] which is more compact and features larger nominal cooling capacity. The heat transfer fluid in both devices was water that was flowing in three separated loops controlled by a series of pumps and solenoid valves. The two systems are large (frame dimensions are in the order of 0.5 - 1 m) and require significantly large forces ($\sim$ 70 kN) to operate.

On a smaller scale a compact demonstrator with stationary SMA was developed based on Ni-Ti sheet/ribbons that were tensile driven to the martensitic transition[171]. The prototype did not use any heat transfer fluid. In that case both heat sink and heat source were

implemented in the device. It was set up in two levels: the upper level contained the SMA ribbon and the motors for loading and unloading, and the lower level contained two copper blocks that acted as heat source and heat sink. These blocks were moved to make contact with the SMA when it was loaded and unloaded thus enabling heat transfer from the cold source to the heat sink.

In the second category, the SMA element is mobile, and it is cyclically put in contact with static heat exchangers. The first tensile driven device[174] can be considered within this category. It was built as multiple Ni-Ti wires mounted between two non-parallel rotating plates. These wires were moved from the two air streams with static flow direction (considered to be two static heat exchangers). A nicely simple compact miniature prototype was developed based on Ni-Ti and Ni-Ti-Co thin films[170,172]. A free-standing SMA film was placed between a heat source and sink made from copper. The surface of the heat source was flat, whereas the heat sink had a convex surface. The film was periodically moved between the source and the sink surface. The out-of-plane deflection caused by the convex surface of the heat sink induced the martensitic transformation in the SMA film with the release of latent heat and transfer to the sink by conduction. When transferred to the flat heat source, the film cooled down due to the reverse transformation and absorbed heat from the source. Other designs involved dual bridges but the principle of operation was similar. The large surface-to-volume ratio of SMA films allowed for fast heat transfer thus enabling high frequency (around 1 Hz) operation of the device.

Although there are still a number of issues to be improved (fatigue, frequency, heat transfer, etc.), these prototypes demonstrate the possibilities of mechanocaloric effects in solid-state refrigeration. A quantitative comparison of several cooling technologies (other than actual vapor/compression) has recently been been reported[175]. Elastocaloric cooling technologies showed up as the best potentially applicable one for large temperature differences between heat and cold source/sinks. The analysis was based on single-stage devices while active magnetic refrigerator devices were taken for the magnetocaloric case. Active elastocaloric refrigerators have already been proposed[50] and indeed, a successful regenerative device has been reported[176] with a performance that exceeds those of other devices based on the magnetocaloric effect.

XIII. CONCLUDING REMARKS AND OUTLOOK

Thermal effects associated with the application of a stress can be achieved by means of hydrostatic pressure and uniaxial load thereby leading to barocaloric and elastocaloric effects. These effects complement the intensively studied electrocaloric and particularly magnetocaloric counterparts and there is great hope that all these caloric effects will contribute in the development of a future clean and environmentally friendly refrigeration technology where it is expected that each of these caloric effects will find its own niche of applicability. Furthermore, the combination of several effects in materials with multicaloric properties can provide a strategy to overcome some of the limitations inherent to the physical mechanisms behind these effects by improving their thermal response and effective reversibility

In the present review, we have examined the key properties of the most significant mechanocaloric materials reported so far. In the vast majority of the materials the giant effect is associated with the occurence of a phase transition which involves a change in the crystal unit cell. Many of these materials also display either electrocaloric or magnetocaloric effects and are good candidates for multicaloric purposes. On the other hand, giant elastocaloric effects have almost been limited so far to shape-memory alloys which are characterized by a huge shear strain at their martensitic transformation. Within this family, conventional (non-magnetic) alloys seem to be the best candidates due to their enhanced ductility in comparison with magnetic and polar compounds. In addition to crystalline materials, a few polymeric materials have also been reported to exhibit mechanocaloric properties and it is expected that intensive research on this kind of materials will result in the development of materials with good mechanocaloric performance.

Although a detailed comparison of mechanocaloric to magnetocaloric and electrocaloric materials has not been the goal of the present review, it is worth mentioning that the values for entropy and temperature changes for barocaloric and elastocaloric materials are similar (or in some particular materials even larger) than those reported for the best magneto- and electrocaloric materials[9]. Furthermore, the efficiencies and estimated coefficients of perfomance for mechanocaloric materials do also compare well to those for other caloric materials[177,178].

The research in mechanocaloric materials is still in its early stages and there are a number of aspects to be addressed to optimize their performances. Among them, hysteresis (which

is intrinsic of first-order transitions) and fatigue seem to be key issues for implementing materials into devices. While materials cycled by hydrostatic pressure are less affected by fatigue, the implementation of the barocaloric effect in particular devices is still challenging because of the requirement of a fluid transmitting pressure. However, it could be envisaged that this fluid could also be advantageously used as a heat transmitting medium. In contrast, elastocaloric devices can be very simple, particularly at a relatively small scale. From this point of view the use of wires, films and foils opens up the possibility of reducing fatigue. Furthermore, the large surface-to-volume ratio enables fast heat transfer and also requires very low forces to achieve large stresses thereby reducing the detrimental effect of hysteresis. Therefore, elastocaloric effect appears as a promising technology for miniature refrigerators and heat-pumps to be used on lab-on-chip systems or micro cooling in bio-medical technology. It can be envisaged that elastocaloric cooling could be scaled down to the nanoscale by taking advantage of the superelastic response (with associated large latent heat) of SMA nano-pillars[179].

While the giant mechanocaloric materials investigated so far show promising mechanocaloric properties and they deserve intensive research, we anticipate that extending this search to other classes of materials such as organics, metal-organics and others, will open new avenues with enormous potential for the development of future mechanocaloric technologies.

ACKNOWLEDGMENTS

We are indebted to all PhD students, post-doctoral researchers and senior colleagues with whom we have been collaborating for many years on the topics covered in this paper. Particular thanks are due to E. Vives, T. Castán, J.L. Tamarit, X. Moya, R. Romero, M. Barrio, P. Lloveras, E. Stern-Taulats, E. Bonnot, D. González-Alonso, D.E. Soto-Parra, S. Yüce and B. Emre. We also acknowledge financial support from CICyT (Spain), projects No. MAT2013-40590-P and MAT2016-75823-R

---

[1] http://ec.europa.eu/clima/policies/international/negotiations/paris/index_en.htm

[2] J.P. Joule, *Phil. Trans.* **1859**, 149, 91.

[3] C. Rodriguez, L.C. Brown, *Metall. Trans. A* **1980**, 11A, 147.

[4] P. Debye, *Ann. Phys.* **1926**, 81, 1154.

[5] W.F. Giauque, *Amer. Chem. Soc.* **1927**, 49, 1864.

[6] G.V. Brown, *J. Appl. Phys.* **1976**, 47, 3673.

[7] V.K. Pecharsky, K.A. Gschneidner, *Phys. Rev. Lett.* **1997**, 78, 4494.

[8] L. Mañosa, A. Planes, M. Acet, *J. Mater. Chem. A* **2013**, 1, 4925.

[9] X. Moya, S. Kar-Narayan, N.D. Mathur, *Nature Mater.* **2014**, 13, 439.

[10] K. A. Gschneidner, V. K. Pecharsky, A. O. Tsokol, *Rep. Prog. Phys.*, **2005** 68, 1479.

[11] E. Brück, *Magnetocaloric refrigeration at ambient temperature*, Handbook of Magnetic Materials, ed. By K.H.J. Buschow, Vol. 17, Elsevier Science, Amsterdam 2008, pp. 235-291.

[12] V. Franco, J.S. Blázquez, B. Ingale, A. Conde, *Annual Rev. Mater. Res.*, **2012**, 42, 305.

[13] A. Smith , C. R. H. Bahl, R. Bjørk , K. Engelbrecht, K. K. Nielsen, N. Pryds *Adv. Ener. Mater.*, **2012**, 2, 1288.

[14] J. F. Scott, *Annual Rev. of Mater. Research*, **2011**, 41, 229.

[15] M. Valant, *Prog. Mater. Sci.*, **2012**, 57, 980.

[16] B. Lu, J. Liu, *Sci. Bull.*, **2015**, 60, 1638.

[17] L. Mañosa, A. Planes, *Philos. Trans. Royal Soc. A*, **2016**, 374, 20150310.

[18] Energy Savings Potential and RD&D Opportunities for Non-Vapor-Compression HVAC Technologies, *Report of the U.S. Dpt. of Energy*, March 2014 (http://energy.gov/eere/buildings/downloads/non-vapor-compressive-hvac-technologies-report).

[19] S. A. Nikitin, K.P. Skokov, Yu S.Koshkidko, Yu G. Pastushenkov, T. I. Ivanova, *Phys. Rev. Lett.*, **2010**, 105, 137205.

[20] M. Balli, S. Jandl, P. Fournier, M. M. Gospodinov, *Appl. Phys. Lett.* **2014**, 104, 232402.

[21] K.F. Wang, J.M. Liu, Z.F. Ren, *Adv. Phys.* **2009**, 58, 321,

[22] M. M. Vopson, *J. Phys. D: Appl. Phys.*, **2013**, 46, 345304.

[23] A. Planes, T. Castán, A. Saxena, *Philos. Mag.* **2014**, 94, 1893.

[24] Volume (strictly speaking not a ferroic property) has a tendency to be minimum at the ground state.

[25] T. Krenke, E. Duman, M. Acet, E. F. Wassermann, X. Moya, L. Mañosa, A. Planes, *Nature Mater.*, **2005**, 4, 450.

[26] A. Planes, L. Mañosa, M. Acet, *J. Phys.: Condens. Matter.* **2009**, 21, 233201.

[27] D. Matsunami, A. Fujita, K. Takenaka, M. Kano, *Nature Mater.*, **2014**, 1, 73.

[28] L.D. Landau and E.M. Lifshitz, *Theory of Elasticity* 2n. Edition **1970**, Pergamon Press. Oxford (UK).

[29] E. Bonnot, R. Romero, L. Mañosa, E. Vives, A. Planes, *Phys. Rev. Lett.* **2008**, 100, 125901.

[30] E. Vives, D. Soto-Parra, L. Mañosa, R. Romero, A. Planes, *Phys. Rev. B* **2009**, 80, 180101(R).

[31] This Maxwell relation is not included in the set given by eq. 3. It results when the fundamental equation is written in terms of the Helmholtz free energy, $\mathcal{F} = U - TS$.

[32] The response to a uniaxial stress combines pure shear and pure volume deformation modes.

[33] M. Porta, T. Castán, P. Lloveras, T. Lookman, A. Saxena, S. R. Shenoy, *Phys. Rev. B*, **2009**, 79, 214117.

[34] O. V. Salman, A. Finel, R. Delville, D. Scryvers, *J. Appl. Phys.*, **2012**, 103517 (2012).

[35] G. Porcari, S. Fabbrici, C. Pernechele, F. Albertini, M. Buzzi, A. Paoluzi, J. Karamad, Z. Arnold, M. Solzi, *Phys. Rev. B*, **2012**, 85, 024414.

[36] E. Stern-Taulats, P.O. Castillo-Villa, L. Mañosa, C. Frontera, S. Pramanick, S. Majumdar, A. Planes, *J. Appl. Phys.* **2014**, 115, 173907.

[37] I. Titov, M. Acet, M. Farle, D. Gonzàlez-Alonso, L. Mañosa, A. Planes, and T. Krenke, *J. Appl. Phys.*, **2012**, 212, 073914.

[38] F. Casanova, A. Labarta, X. Batlle, F.J. Pérez-Reche, E. Vives, L. Mañosa, A. Planes, *Appl. Phys. Lett.* **2005**, 86, 262504.

[39] X. Moya, E. Stern-Taulats, S. Crossley, D. Gonzàlez-Alonso, S. Kar-Narayan, A. Planes, L. Mañosa, N.D. Mathur, *Adv. Mater.* **2013**, 25, 1360.

[40] *Shape Memory Alloys* (Eds. K. Otsuka, C.M. Wayman), Cambridge University Press, Cambridge **1998**.

[41] A. Planes, L. Mañosa, *Solid State Phys.* **2001**, 55, 159.

[42] L. Mañosa, A. Planes, J. Ortín, B. Martínez, *Phys. Rev. B* **1993**, 48, 3611.

[43] R. Kuentzler, *Sol. State Comm.* **1992**, 989.

[44] M. Ahlers, *Prog. Mat. Sci.* **1986**, 30, 135.

[45] L. Mañosa, A. Planes, E. Vives, E. Bonnot, R. Romero, *Funct. Mater. Lett.* **2009**, 2, 73.

[46] E. Vives, S. Burrows, R.S. Edwards, S. Dixon, L. Mañosa, A. Planes, R. Romero, *Appl. Phys. Lett.* **2011**, 98, 011902.

[47] E. Vives, L. Mañosa, A. Planes. Unpublished.

[48] E. Vives, J. Ortín, L. Mañosa, I. Ràfols, R. Pérez-Magrané, A. Planes, *Phys. Rev. Lett.* **1994**, 72, 1694.

[49] L. Mañosa, S. Jarque-Farnos, E. Vives, A. Planes, *Appl. Phys. Lett.* **2013**, 103, 211904.

[50] J. Tusek, K. Engelbrecht, R. Millán-Solsona, L. Mañosa, E. Vives, L.P. Mikkelsen, N. Pryds, *Adv. Energy Mater.* **2015**, 5, 1500361.

[51] K. Otsuka, X. Ren, *Prog. Mat. Sci.* **2005**, 50, 511.

[52] J. Quarini, A. Prince, *J. Mechanical Engineering Sci.* **2004**, 218, 1175.

[53] G.J. Pataky, E. Ertekin, H. Sehitoglu, *Acta Mater.* **2015**, 96, 420.

[54] J. Cui, Y. Wu, J. Muehlbauer, Y. Hwang, R. Radermacher, S. Fackler, M. Wuttig, I. Takeuchi, *Appl. Phys. Lett.* **2012**, 101, 073904.

[55] J. Tusek, K. Engelbrecht, L.P. Mikkelsen, N. Pryds, *J. Appl.Phys.* **2015**, 117, 124901.

[56] E.A. Pieczyska, H. Tobushi, K. Kulasinski, *Smart Mater. Struct.* **2013**, 22, 035007.

[57] H. Ossmer, F. Lambrecht, M. Gueltig, C. Chluba, E. Quandt, M. Kohl, *Acta Mater.* **2014**, 81, 9.

[58] H.Ossmer, S. Miyazaki, M. Kohl, *Mater. Today: Proc.* **2015**, 2S, S971.

[59] H. Ossmer, C. Chluba, M. Gueltig, E. Quandt, M. Kohl, *Shap. Mem. Superel.* **2015** 1, 142

[60] D. Soto-Parra, E. Vives, L. Mañosa, J.A. Matutes-Aquino, H. Flores-Zuñiga, A. Planes, *Appl. Phys. Lett.* **2016**, 108, 071902.

[61] M. Schmidt, J. Ullrich, A. Wieczorek, J. Frenzel, A. Schütze, G. Eggeler, S. Seelecke, *Shap. Mem. Superelasticity* **2015**, 1, 132.

[62] S. Sarkar, X. Ren, K. Otsuka, *Phys. Rev. Lett.* **2005**, 95, 205702.

[63] Z. Tang, Y. Wang, X.Liao, D. Wang, S. Yang, X. Song, *J. Alloys and Compd.* **2015**, 622, 622.

[64] C. Bechtold, C. Chluba, R. Lima de Miranda, E. Quandt, *Appl. Phys. Lett.* **2012**, 101, 091903.

[65] C. Chluba, H. Ossmer, C. Zamponi, M. Kohl, E. Quandt, *Shap. Mem. Superelasticity* **2016**, 2, 95.

[66] C. Chluba, W. Ge, R. Lima de Miranda, J. Strobel, L. Kienle, E. Quandt, M. Wuttig, *Science* **2015**, 348, 1004.

[67] F. Xiao, T. Fukuda, T. Kakeshita, *Scripta Mater.* **2016**, 124, 133.

[68] G. Shirane, R. Nathans, C.W. Chen, *Phys. Rev.* **1964**, 134 A1547.

[69] A.X. Gray, D.W. Cooke, P. Krüger, C. Bordel, A.M. Kaiser, S. Moyerman, E.E. Fullerton, S. Ueda, Y. Yamashita, A. Gloskovskii, C.M. Schneide, W. Drube, K. Kobayashi, F. Hellman,

C.S. Fadley, *Phys. Rev. Lett.* **2012**, 108, 257208.

[70] D.W. Cooke, F. Hellman, C. Baldasseron, C. Bordel, S. Moyerman, E.E. Fullerton, *Phys. Rev. Lett.* **2012**, 109, 255901.

[71] J.B. Staunton, R. Banerjee, M. dos Santos Dias, A. Deak, L. Szunyogh, *Phys. Rev. B* **2014**, 89, 054427.

[72] S. Nikitin, G. Myalikgulyev, A.M. Tishin, M.P. Annaorazov, K.A. Asatryan, A.L. Tyurin, *Phys. Lett.* **1990**, 148, 363.

[73] S. Nikitin, G. Myalikgulyev, M.P. Annaorazov, A.L. Tyurin, R.W. Myndev, S.A. Akopayan, *Phys. Lett.* **1992**, 171, 234.

[74] E. Stern-Taulats, A. Planes, P. Lloveras, M. Barrio, J.L. Tamarit, S. Pramanick, S. Majumdar, C. Frontera, L. Mañosa, *Phys. Rev. B* **2014**, 89, 214105.

[75] E. Stern-Taulats, A. Gràcia-Condal, A. Planes, P. Lloveras, M. Barrio, J.L. Tamarit, S. Pramanick, S. Majumdar, L. Mañosa, *Appl. Phys. Lett.* **2015**, 107, 152409.

[76] A. Chirkova, K.P. Skokov, L. Schultz, N.V. Baranov, O. Gutfleisch, T.G. Woodcock, *Acta Mater.* **2016**, 106, 15.

[77] B.G. Shen, J.R. Sun, F.X. Hu, H.W. Zhang, Z.H. Cheng, *Adv. Mater.* **2009**, 21, 4545.

[78] M. E. Gruner, W. Keune, B. Roldan Cuenya, C. Weis, J. Landers, S.I. Makarov, D. Klar, M.Y. Hu, E.E. Alp, J. Zhao, M. Krautz, O. Gutfleisch, H. Wende, *Phys. Rev. Lett.* **2015**, 114, 057202.

[79] L. Mañosa, D. González-Alonso, A. Planes, M. Barrio, J.L. Tamarit, I.S. Titov, M. Acet, A. Bhattacharyya, S. Majumdar, *Nature Comm.* **2011** 2, 595.

[80] D. Matsunami, A. Fujita, K. Takenaka, M. Kano, *Nature Mater.* **2015**, 14, 73.

[81] J. García, J. Bartolomé, D. González, *J. Chem. Thermodynamics* **1983**, 15, 1041.

[82] W. Choe, V.K. Pecharsky, A.O. Pecharsky, K.A. Gschneidner Jr, V.G. Young Jr, G.J. Miller, *Phys. Rev. Lett.* **2000**, 84, 4617.

[83] F. Casanova, X. Batlle, A. Labarta, J. Marcos, L. Mañosa, A. Planes, *Phys. Rev. B* **2002**, 66, 212402.

[84] S. Yüce, M. Barrio, B. Emre, E. Stern-Taulats, A. Planes, J.L. Tamarit, Y. Mudryk, K.A. Gschneidner Jr., V.K. Pecharsky, L. Mañosa, *Appl. Phys. Lett.* **2012**, 101, 071906.

[85] N.T. Trung, L. Zhang, L. Caron, K.H.J. Buschow, E. Brück, *Appl. Phys. Lett.* **2010** 96, 172504.

[86] R.R. Wu et al., *Sci. Reports* **2015**, 5, 18027.

[87] T. Samanta, P. Lloveras, A.U. Saleheen, D.L. Lepowski, E. Kramer, I. Dubenko, P.W. Adams, D.P. Young, M. Barrio, J.L. Tamarit, N. Ali, S. Stadler, *arxiv:1602.07584* **2016**.

[88] T. Kakeshita, K. Ullakko, *MRS Bull.* **2002**, 27, 105.

[89] F. Xiao, T. Fukuda, T. Kakeshita, *Appl. Phys. Lett.* **2013**, 102, 161914.

[90] F. Xiao, T. Fukuda, T. Kakeshita, X. Jin, *Acta Mater.* **2015**, 87, 8.

[91] F. Xiao, T. Fukuda, T. Kakeshita, *Philos. Mag.* **2015**, 95 1390.

[92] F. Xiao, X. Liang, X. Jin, Z. Nie, T. Kakeshita, T. Fukuda, *Acta Mater.* **2016**, 118, 88.

[93] M. Acet, L. Mañosa, A. Planes, *Handbook of Magnetic Material* **2011** 19, 231.

[94] S. Kaufmann, U.K. Rossler, O. Heczko, M. Wuttig, J. Buschbeck, L. Schultz, S. Fahler, *Phys. Rev. Lett.* **2010**, 104, 145702.

[95] S. Singh, V. Petricek, P.Rajput, A.H. Hill, E. Suard, S.R. Barman, D. Pandey, *Phys. Rev. B* **2014** 90, 014109.

[96] R. Kainuma, Y. Imano, W. Ito, Y. Sutou, H. Morito, S. Okamoto, O. Kitakami, K. Oikawa, A. Fujita, T. Kanomata, K. Ishida, *Nature* **2006**, 439 957.

[97] T. Krenke, E. Duman, M. Acet, E.F. Wassermann, X. Moya, L. Mañosa, A. Planes, E. Suard, B. Ouladdiaf, *Phys. Rev. B* **2007**, 75, 104414.

[98] V.V. Khovaylo, T. Kasomata, T. Tanaka, M. Nakashima, Y. Amako, R. Kainuma, R.Y. Umetsu, H. Morito, H. Miki, *Phys. Rev. B* **2009**, 80, 144409.

[99] K. Ollefs, Ch. Schöppner, I. Titov, R. Meckenstock, F. Wilhelm, A. Rogalev, J. Liu, O. Gutfleisch, M. Farle, H. Wende, M. Acet, *Phys. Rev. B* **2015**, 92, 224429.

[100] S. Aksoy, M. Acet, P.P. Deen, L. Mañosa, A. Planes, *Phys. Rev. B* **2009**, 79, 212401.

[101] L. Mañosa, X. Moya, A. Planes, O. Gutfleisch, J. Lyubina, M. Barrio, J.L. Tamarit, S. Aksoy, T. Krenke, M. Acet, *Appl. Phys. Lett.* **2008**, 92, 012515.

[102] V. Recarte, M. Zbiri, M. Jiménez-Ruiz, V. Sánchez-Alarcos, J. I. Pérez-Landazábal, *J. Phys.: Condens. Matter* **2016**, 28, 205402.

[103] L. Mañosa, A. Planes, J. Zarestky, T. Lograsso, D.L. Schlagel, C. Stassis, *Phys. Rev. B* **2001**, 64, 024305.

[104] X. Moya, D. González-Alonso, L. Mañosa, A. Planes, V.O. Garlea, T.A. Lograsso, D.L. Schlagel, J.L. Zarestky, S. Aksoy, M. Acet, *Phys. Rev. B 2009* 79, 214118

[105] T. Kihara, X. Xu, W. Ito, R. Kainuma, M. Tokunaga, *Phys. Rev. B* **2014**, 90, 214409.

[106] D.E. Soto-Parra, E. Vives, D. González-Alonso, L. Mañosa, A. Planes, R. Romero, J.A.

Matutes-Aquino, R.A. Ochoa-Gamboa, H. Flores-Zúñiga, *Appl. Phys. Lett.* **2010**, 96, 071912.

[107] P.O. Castillo-Villa, D.E. Soto-Parra, J.A. Matutes-Aquino, R.A. Ochoa-Gamboa, A. Planes, L. Mañosa, D. González-Alonso, M. Stipcich, R. Romero, D. Ríos-Jara, H. Flores-Zúñiga, *Phys. Rev. B* **2011**, 83, 174109.

[108] Y. Xu, B. Lu, W. Sun, A. Yan, J. Liu, *Appl. Phys. Lett.* **2015**, 106, 201903.

[109] Y. Li, D. Zhao, J. Liu, *Sci. Reports* **2016** 6, 25500.

[110] F. Xiao, M. Jin, J. Liu, X. Jin, *Acta Mater.* **2015** 96, 292.

[111] P.O. Castillo-Villa, L. Mañosa, A. Planes, D. E. Soto-Parra, J.L. Sánchez-Llamazares, H. Flores-Zúñiga, C. Frontera, *J. Appl. Phys.* **2013**, 113, 053506.

[112] R. Millán-Solsona, E. Stern-Taulats, E. Vives, A. Planes, J. Sharma, A. K. Nayak, K.G. Suresh, L. Mañosa, *Appl. Phys. Lett.* **2014**, 105, 241901.

[113] Z. Yang, D.Y. Cong, L. Huang, Z.H. Nie, X.M. Sun Q.H. Zhang, Y.D. Wang, *Mater. and Design* **2016** 92, 932.

[114] W. Sun, J. Liu, B. Lu, Y. Li, A. Yan, *Scripta Mater.* **2016**, 114, 1.

[115] B. Lu, F. Xiao, A. Yan, J. Liu, *Appl. Phys. Lett.* **2014**, 105, 161905.

[116] B. Lu, P. Zhang, Y. Xu, W. Sun, J. Liu, *Mater. Lett.* **2015**, 148, 110.

[117] Y.J. Huang, Q.D. Hu, N.M. Bruno, J.H. Chen, I. Karaman, J.H. Ross Jr., J.G. Li, *Scripta Mater.* **2015**, 105, 42.

[118] E. Şaşıoğlu, L. M. Sandratskii, P. Bruno, *Phys. Rev. B* **2005**, 71, 214412.

[119] V. D. Buchelnikov, P. Entel, S. V. Taskaev, V. V. Sokolovskiy, A. Hucht, M. Ogura, H. Akai, M. E. Gruner, S. K. Nayak, *Phys. Rev. B* **2008**, 78, 184427.

[120] K.A. Müller, F. Fauth, S. Fischer, M. Koch, A. Furrer, P. Lacorre, *Appl. Phys. Lett.* **1998**, 73, 1056.

[121] L. Mañosa, D. González-Alonso, A. Planes, E. Bonnot, M. Barrio, J.L. Tamarit, S. Aksoy, M. Acet, *Nature Mater.* **2010**, 9, 478.

[122] E. Stern-Taulats, A. Planes, P. Lloveras, M. Barrio, J.L. Tamarit, S. Pramanick, S. Majumdar, S. Yüce, B. Emre, C. Frontera, L. Mañosa, *Acta Mater.* **2015**, 96, 324.

[123] S. Fabbrici, F. Albertini, A. Paoluzi, F. Bolzoni, R. Cabassi, M. Solzi, L. Righi, G. Calestani, *Appl. Phys. Lett.* **2009**, 95, 022508.

[124] L. Mañosa, E. Stern-Taulats, A. Planes, P. Llovera, M. Barrio, J.L. Tamarit, B. Emre, S. Yüce, S. Fabbrici, F. Albertini, *phys. stat. sol. (b)* **2014**, 251, 2114.

[125] *Physics of Crystalline Dielectrics* Ed. by I.S. Zheludev , Springer **1971**.

[126] F. Jona, G. Shirane, *Ferroelectric Crystals* Pergamon Press. Oxford **1962**.

[127] E. Stern-Taulats, P. Llovera, M. Barrio, E. Defay, M. Egilmez, A. Planes, J.L. Tamarit, L. Mañosa, N.D. Mathur, X. Moya, *APL Materials* **2016**, in press.

[128] E.A. Mikhaleva, I.N. Flerov, M.V. Gorev, M.S. Molokeev, A.V. Cherepakhin, A.V. Kartashev, N.V. Mikhasenok, K.A. Sablina, *Phys. Sol. State* **2012**, 54, 1719.

[129] D. O'Reilly, T. Tsang, *J. Chem. Phys.* **1967**, 46, 1291.

[130] U. Dahlborg, K.E. Larsson, E. Pirkmajer, *Physica* **1970**, 49, 1.

[131] P. Lloveras, E. Stern-Taulats, M. Barrio, J.L. Tamarit, S. Crossley, W. Li, V. Pomjakushin, A. Planes, L. Mañosa, N.D. Mathur, X. Moya, *Nature Comm.* **2015**, 6, 8801.

[132] R.L. Withers, F.J. Brink,. Y. Liu, L. Noren, *Polyhedron* **2007**, 26, 290.

[133] M. Gorev, E. Bogdanov, I. Flerov, N. Laptash, *J. Phys.: Condens. Matter* **2010**, 22, 185901.

[134] M.V. Gorev, E.V. Bogdanov, I.N. Flerov, A.G. Kocharova, N.M. Laptash, *Phys. Solid State* **2010**, 52, 167.

[135] I.N. Flerov, A.V. Kartashev, M.V. Gorev, E.V. Bogdanov, S.V. Mel'nikova, M.S. Molokeev, E.I. Pogoreltsev, N.M. Laptash, *J. Fluorine Chem.* **2016**, 183, 1.

[136] M.V. Gorev, I.N. Flerov, E.V. Bogdanov, V.N. Voronov, N.M. Laptash, *Phys. Solid State* **2010**, 52, 377.

[137] S. Linsekov, I. Ponomareva, *Phys. Rev. B* **2012**, 86, 104103.

[138] S. Linsekov, B.K. Mani, C.-M. Chang, J. Amand, I. Ponomareva, *Phys. Rev. B* **2013**, 87, 224101.

[139] J.A. Barr, S.P. Beckman, T. Nishimatsu, *J. Phys. Soc. Japan* **2015**, 84, 024716.

[140] Y. Liu, I.C. Infante, X. Lou, L. Bellaiche, J.F. Scott, B. Dkhil, *Adv. Mater.* **2014**, 26, 6132.

[141] Y. Liu, J. Wei, P.E. Janolin, I.C. Infante, J. Kreisel, X. Lou, B. Dkhil, *Phys. Rev. B*, **2014**, 90, 104107.

[142] A. Chauhan, S. Patel, R. Vaish, *Acta Mater.* **2015**, 89, 384.

[143] A. Chauhan, S. Patel, R. Vaish, *Appl. Phys. Lett.* **2015**, 106, 172901.

[144] S. Patel, A. Chauhan, R. Vaish, *Energy Technology* **2016** doi: 10.1002/ente.201500446.

[145] E. Stern-Taulats, L. Mañosa, A. Planes, unpublished.

[146] D. Guyomar, Y. Li, G. Sebald, P.J. Cottinet, B. Ducharne, J.F. Capsal, *Appl. Thermal Eng.*, **2013**, 57, 33.

[147] Z. Xie, G. Sebald, D. Guyomar, *Appl. Phys. Lett.*, **2015**, 107, 081905.

[148] Z. Xie, G. Sebald, D. Guyomar, *Appl. Phys. Lett.*, **2016**, 108, 041901.

[149] Z. Xie, G. Sebald, D. Guyomar, *arxiv.* **2016**.

[150] S.L. Dart, R.L. Anthony, E. Guth, *Ind. Eng. Chem.*, **1942**, 34, 1340.

[151] B. Neese, B. Chu, S.G. Lu, Y. Wang, E. Furman, Q.M. Zhang, *Science*, **2008**, 321, 821.

[152] C.M. Roland, J.T. Garret, R. Casalini, D.F. Roland, P.G. Santangelo, S.B. Qadri, *Chem. Mater.*, **2004**, 16, 857.

[153] S. Patel, A. Chahan, R. Vaish, P. Thomas, *Appl. Phys. Lett.* **2016**, 108, 072903.

[154] Y. Yoshida, K. Yuse, D. Guyomar, J.F. Capsal, G. Sebald, *Appl. Phys. Lett.* **2016**, 108, 242904.

[155] E.L. Rodriguez, F.E. Filisko, *J. Appl. Phys.* **1982**, 53, 6536.

[156] S. Gama, A. A. Coelho, A. de Campos, A. Magnus, G. Carvalho, F. C. G. Gandra, P. J. von Ranke, N. A. de Oliveira, *Phys. Rev. Lett.*, **2004**, 93, 237202.

[157] G. J. Liu, J. R. Sun, J. Shen, B. Gao, H. W. Zhang, F. X. Hu, B. G. Shen, *Appl. Phys. Lett.*, **2007**, 90, 032507.

[158] L. Caron, Z. Q. Ou, T. T. Nguyen, D. T. Cam Thanh, O. Tegus, E. Brück, *J. Mag. Mag. Mater.*, **2007**, 321, 3559.

[159] L. Morellon, Z. Arnold, P. A. Algarabel, C. Magen, M. R. Ibarra,Y. Skorokhod, *J. Phys.: Condens. Matter, **2004**, 16 1623.*

[160] A. Magnus, G. Carvalho, C. S. Alves, A. de Campos, A. A. Coelho, S. Gama, F. C. G. Gandra, P. J. von Ranke, N. A. Oliveira, *J. Appl. Phys.*, **2005**, 97, 10M320.

[161] J. Lyubina, K. Nenkov, L. Schulta, O. Gutfleisch, *Phys. Rev. Lett.* **2008**, 101, 177203.

[162] L. Caron, N. T. Trung, E. Brück, *Phys. Rev. B*, **2011**, 84, 020414(R).

[163] T. Samanta, L. Lepkowski, A. U. Saleheen, A. Shankar, J. Prestigiacomo, I. Dubenko, A. Quetz, I. W. H. Oswald, G. T. McCandless, J. Y. Chan, P. W. Adams, D. P. Young, N. Ali, S. Stadler, *Phys. Rev. B*, **2015**, 91. 020401(R).

[164] A. K. Nayak, K. G. Suresh, A. K. Nigam, A. A.Coelho, S. Gama, *J. Appl. Phys.*, **2009**, 106, 053901.

[165] J. Liu, T. Gottschall, K. P. Skokov, J. D. Moore, O. Gutfleisch, *Nature Mater.*, **2012**, 11, 620.

[166] A. Planes, T. Castán, A. Saxena, *Philos. Trans. Roy. Soc. A*, **2016**, 374, 20150304.

[167] S. Lisenkov, B. K. Mani, C.-M. Chang, J. Almand, I. Ponomareva, *Phys. Rev. B*, **2013**, 87, 224101.

[168] S. Qian, Y. Wu, J. Ling, J. Muehlbauer, Y. Hwuang, I. Takeuchi, R. Radermacher, *International Congress on Refrigeration*, **2015**, Paper 0092.

[169] S. Qian, Y. Geng, Y. Wang, J. Muehlbauer, J. Ling, Y. Hwang, R. Radermacher, I. Takeuchi, *Science and Tech. for the Built Environment* **2016** DOI:10.1080/23744731.2016.1171630.

[170] H. Ossmer, S. Miyazaki, M. Kohl, *Transducers*, **2015**, Anchorage, USA, DOI: 10.1109/TRANSDUCERS.2015.7181026.

[171] M. Schmidt, A. Schütze, S. Seelecke, *Int. J. Refrig.*, **2015**, 54, 88.

[172] H. Ossmer, C. Chluba, S. Kaufmann-Weiss, E. Quandt, M. Kohl, *APL Mater.*, **2016**, 4, 064102.

[173] M. Schmidt, S.M. Kirsch, S. Seelecke, A. Schütze, *Science and Tech. for the Built Environment* **2016** DOI:10.1080/23744731.2016.1186423.

[174] S. Qian, Y. Geng, Y. Wang, J. Ling, Y. Hwang, R. Radermacher, I. Takeuchi, J. Cui, *Int. J. Refrig.*, **2016**, 64, 1.

[175] S. Qian, D. Nasut, A. Rhoads, Y. Wang, Y. Geng, Y. Hwang, R. Radermacher, I. Takeuchi, *Int. J. Refrig.*, **2016**, 62 177.

[176] J. Tusek, K. Engelbrecht, D. Eriksen, S. Dall'Olio, J. Tusek, N. Pryds, *Nature Energy* **2016**. In press.

[177] S. Crossley, N.D. Mathur, X. Moya, *AIP Advances* **2015**, 5, 067153.

[178] I. Takeuchi, K. Sandeman, *Mater. Today* **2015**, 62, 48.

[179] J. San Juan, M.L. No, C. A. Schuh, *Adv. Mater.* **2008**, 20, 272.

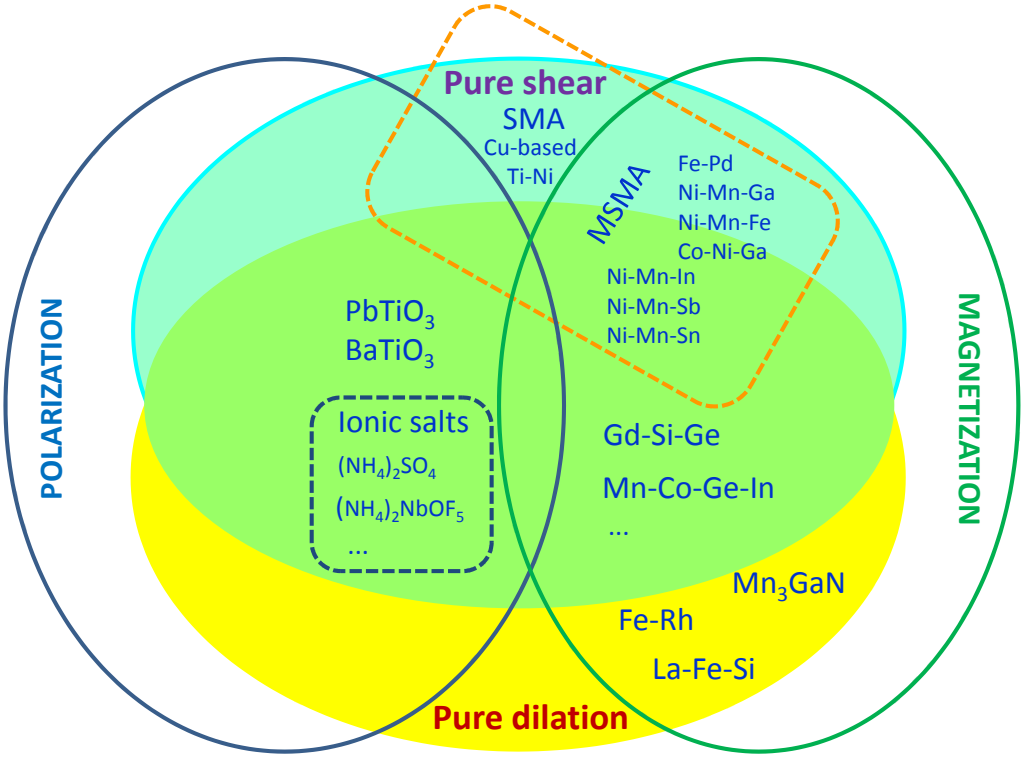

FIG. 1. Classification of the diverse giant mechanocaloric materials in terms of the unit cell distortion at the structural transition, and coupling between structural and other (magnetic, polar) degrees of freedom.

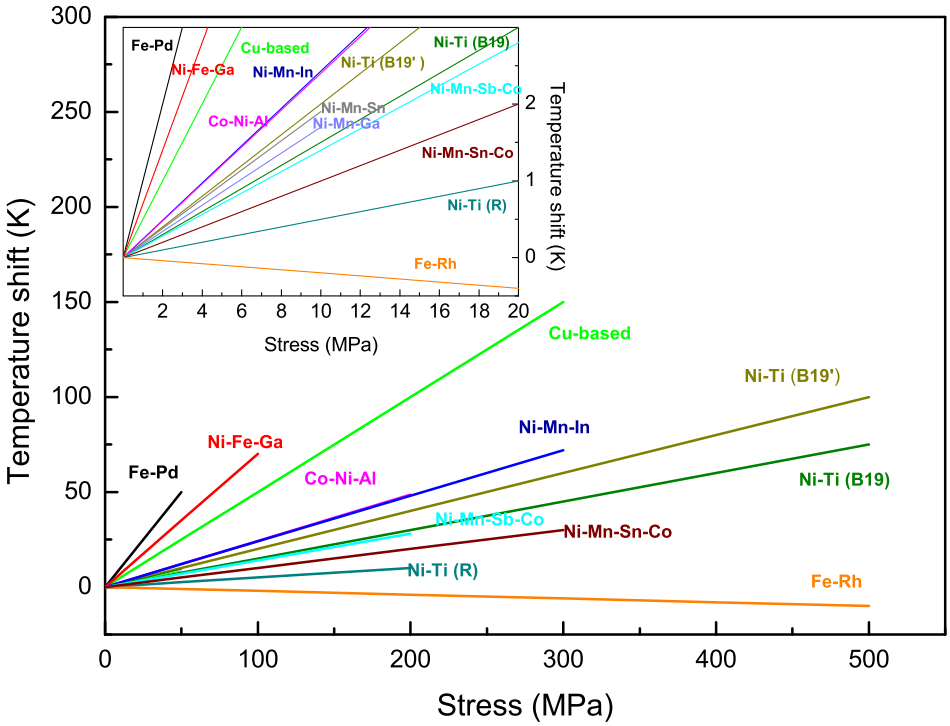

FIG. 2. Shift in the transition temperature as a function of applied uniaxial stress. The inset shows an enlarged view of the low stress region. The length of the lines is indicative of the maximum stress applied to each material. The same color code has been used to identify the different materials in all figures.

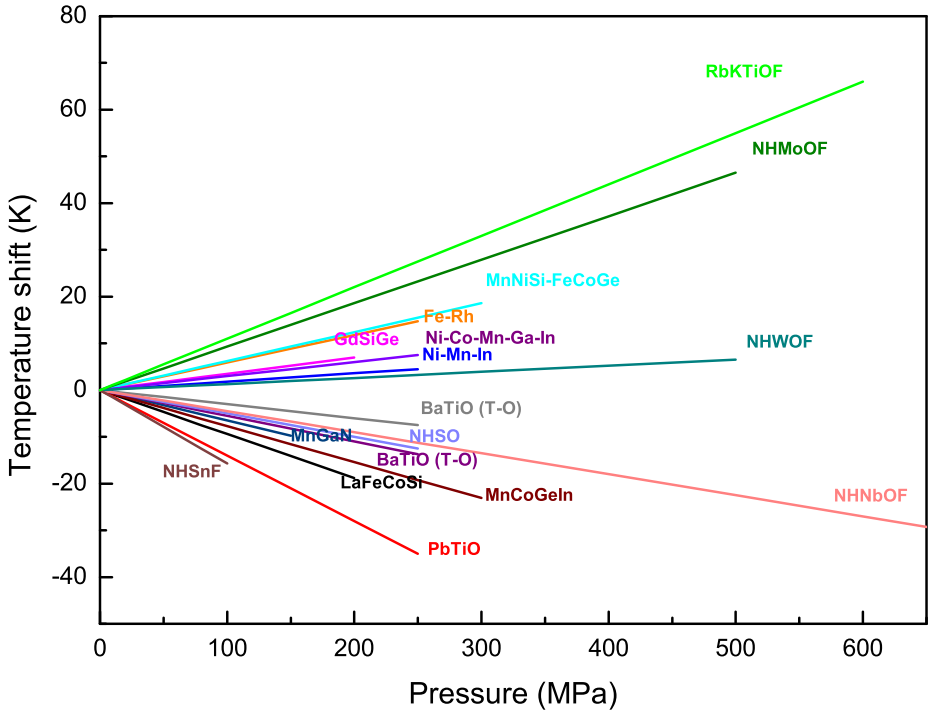

FIG. 3. Shift in the transition temperature as a function of hydrostatic pressure. The length of the lines is indicative of the maximum stress applied to each material. The same color code has been used to identify the different materials in all figures.

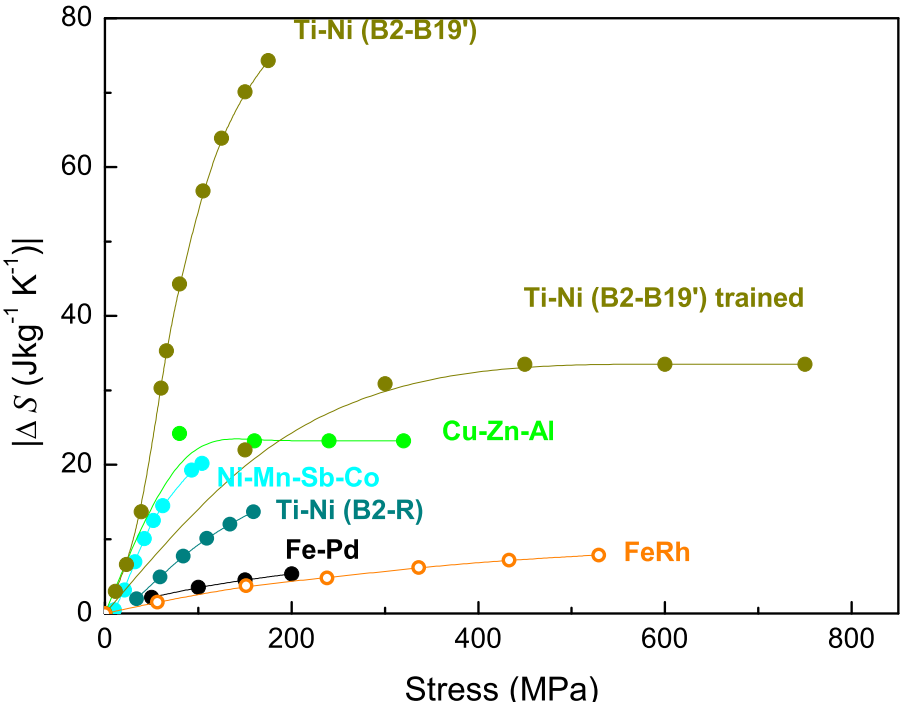

FIG. 4. Absolute value for the isothermal entropy change as a function of the applied uniaxial stress for selected giant elastocaloric materials. Solid symbols stand for quasi-direct data and open symbols correspond to data estimated from temperature measurements. The same color code has been used to identify the different materials in all figures.

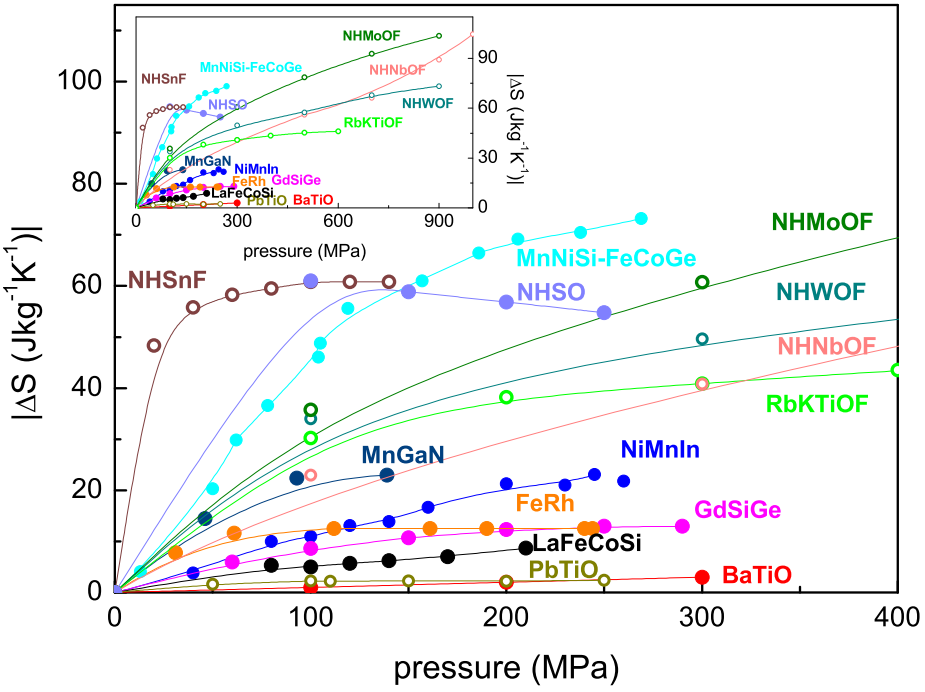

FIG. 5. Absolute value for the isothermal entropy change as a function of the applied hydrostatic pressure for selected giant barocaloric materials. Solid symbols stand for quasi-direct measurements and open symbols represent improper quasi-direct methods (see text for details). The inset shows an extended view up to high values of pressure. The same color code has been used to identify the different materials in all figures.

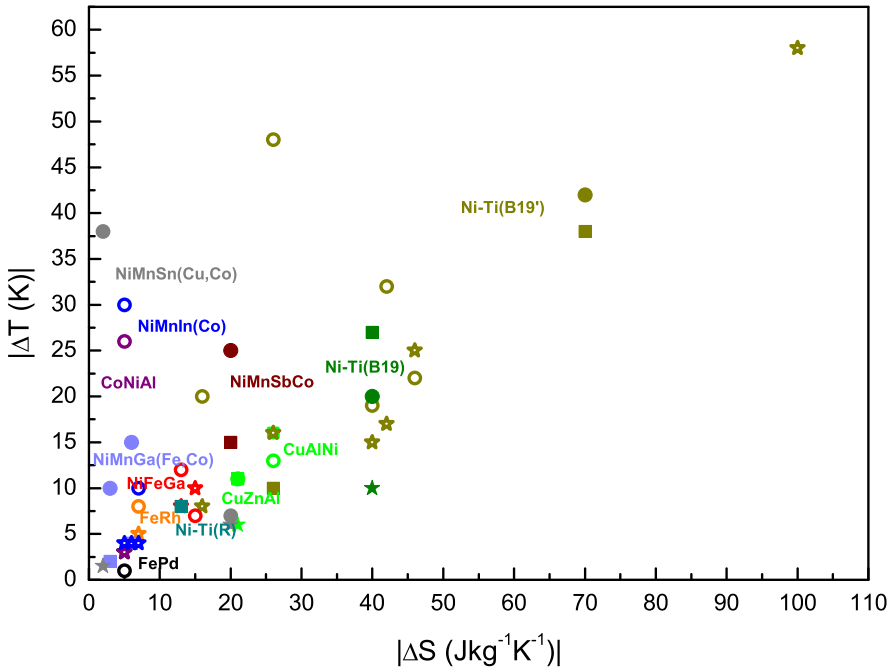

FIG. 6. Absolute value for the adiabatic temperature change as a function of the absolute value of the isothermal entropy change for selected giant elastocaloric materials. Solid symbols stand for indirect measurements of the entropy change and open symbols represent entropy values estimated from measured temperature changes. For the adiabatic temperature change: Stars correspond to direct measurements; squares, to estimated values; and circles, to values derived from the transition entropy change. The same color code has been used to identify the different materials in all figures.

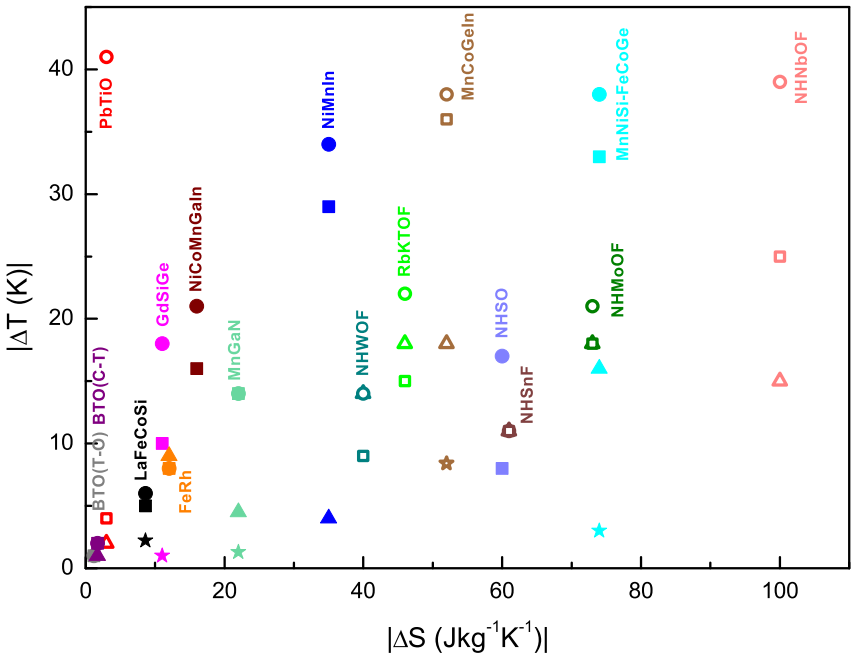

FIG. 7. Absolute value for the adiabatic temperature change as a function of the absolute value of the isothermal entropy change for selected giant barocaloric materials. Solid symbols stand for quasi-direct measurements of the entropy change and open symbols stand for improper quasi-direct methods of the entropy change (see text for details). For the adiabatic temperature change: Stars correspond to direct measurements; triangles, to quasi-direct measurements; squares, to estimated values; and circles, to values derived from the transition entropy change. The same color code has been used to identify the different materials in all figures.

Compound	Crystallographic change	C ($Jkg^{-1}K^{-1}$)	ρ (kgm^{-3})	T_t (K)	ε %	ΔS_t ($Jkg^{-1}K^{-1}$)	ΔT_t (K)	$dT/d\sigma$ (10^{-3} $KMPa^{-1}$)	Δσ (MPa)	ΔS^i ($Jkg^{-1}K^{-1}$)	ΔS^e ($Jkg^{-1}K^{-1}$)	ΔT^d (K)	ΔT^e (K)	Reference
$Cu_{68.13}Zn_{15.74}Al_{16.13}$ (sc)	C(*Fm3m*)-M(*C/2m*)	430	7700	230	8	21	11	500	120	20.7	11	6	11	29,46
$Cu_{68}Zn_{16}Al_{16}$	C(*Fm3m*)-M(*C/2m*)	430	7700	200	7	18	8	500	50	18	13	6	8	49
$Cu_{83}Al_{14}Ni_3$ (sc)	C(*Fm3m*)-M(*C/2m*)	410	7600	250	8	21	13	500	150	-	26	16	-	3
$Ni_{50.38}Ti_{49.62}$ (sc)	C(*Pm3m*)-M(*P2/m*)	590	7600	220	5	42-50	16-19	125	500	-	40	15	-	53
$Ni_{48.7}Ti_{51.3}$	C(*Pm3m*)-M(*P2/m*)	550	6450	220	8	-	-	-	300	26	-	-	10	63
$Ni_{50}Ti_{50}$ (wire)	C(*Pm3m*)-M(*P2/m*)	550	6500	300	8	40	22	-	500	-	46	25	-	54
$Ni_{48.9}Ti_{51.1}$ (wire)	C(*Pm3m*)-M(*P2/m*)	550	6500	300	5	-	-	133	800	-	46	25	-	55
$Ni_{47.9}Ti_{52.6}$ (wire)	C(*Pm3m*)-M(*P2/m*)	550	6500	300	7	70-80	38-44	200	175	70	-	-	38	60
$Ni_{50}Ti_{50}$ (film)	C(*Pm3m*)-M(*P2/m*)	420	6500	260	3.5	77	48	-	500	-	26	16	-	57
$Ni_{50.5}Ti_{49.5}$ (foil)	C(*Pm3m*)-M(*P2/m*)	500	6500	280	6	-	-	-	1300	-	100	58	-	56
$Ni_{50.5}Ti_{49.1}Fe_{0.4}$ (foil)	C(*Pm3m*)-M(*P2/m*)	500	6500	200	4	80	32	-	500	-	42	17	-	59
$Ni_{45}Ti_{47.25}Cu_5V_{2.75}$	C(*Pm3m*)-M(*P2/m*)	500	6500	250	5	40	20	-	500	-	16	8	-	61
$Ni_{47.9}Ti_{52.6}$ (wire)	C(*Pm3m*)-R(*P3*)	500	6500	310	0.5	18	11	50	175	13	-	-	8	60
$Ti_{59.4}Ni_{32.5}Cu_{12.6}$ (film)	C(*Pm3m*)-O(*Pmmma*)	840(*)	6500	320	1.5	52	20(*)	-	300	-	21(*)	6	-	64
$Ti_{54.7}Ni_{30.7}Cu_{12.3}Co_{2.3}$ (film)	C(*Pm3m*)-O(*Pmmma*)	420	6450	280	1.7	30	20	95	200	40	15	10	27	65
$Fe_{49}Rh_{51}$	C(*Pm3m*)-C(*Pm3m*)	470	9800	310	0.3	13	8	-20	500	-	7	5	-	73
$Fe_{68.8}Pd_{31.2}$ (sc)	C(*Pm-3m*)-T(P4/*mmm*)	400	8900	250	2	1	0.6(#)	1000(#)	200	-	5	3	-	89,90
$Ni_{52.6}Mn_{21.9}Ga_{24.2}Fe_{1.3}$	C(*Fm3m*)-M/T	450	8000	330	3	20	15	165	10	6	-	-	4	106
$Ni_{50.5}Mn_{21.7}Ga_{24.7}Co_{3.1}$	C(*Fm3m*)-M/T	450	7900	270	1.8	16	10	-	10	3	-	-	2	107
$Ni_{54}Fe_{19}Ga_{27}$	C(*Fm3m*)-M/T	470	8450	280	3	11	6	-	170	-	7	4	-	108
$Ni_{54}Fe_{19}Ga_{27}$ (sc)	C(*Fm3m*)-M/T	460	845	280	14	16-20	10-12	300-700	150	-	13	8	-	53,109
$Ni_{50}Fe_{19}Ga_{27}Co_4$ (sc)	C(*Fm3m*)-M/T	450	8500	300	4.5	11	7	400	300	-	15	10	-	110
$Co_{40}Ni_{33.17}Al_{28.63}$	C(*Fm3m*)-M/T	480	7300	290	10	44	26	240	50	-	5	3	-	53
$Ni_{43}Mn_{40}Sn_{10}Cu_7$	C(*Fm3m*)-M/T	450	7900	320	1	54	38	200	10	2	-	-	1.5	111
$Ni_{46}Mn_{38}Sb_{12}Co_4$	C(*Fm3m*)-M/T	400	7700	300	2.5	34	25	130	100	20	-	-	15	112
$Ni_{43.5}Mn_{39}Sn_{11}Co_{6.5}$	C(*Fm3m*)-M/T	500	8050	260	3	14	7	100	300	12	-	-	6	113
$Ni_{45}Mn_{44}Sn_{11}$	C(*Fm3m*)-M/T	580	7900	270	2.3	32	15	-	260	-	13	6	-	114
$Ni_{45.7}Mn_{36.6}In_{13.3}Co_{5.1}$	C(*Fm3m*)-M/T	460	8100	280	1	-	-	-	100	-	6	4	-	115
$Ni_{45}Mn_{36.4}In_{13.6}Co_5$	C(*Fm3m*)-M/T	460	8100	250	3	18	10	-	150	-	7	4	-	116
$Ni_{48.4}Mn_{34.8}In_{16.8}$	C(*Fm3m*)-M/T	400	7150	300	1.5	40	30	240	250	-	5	4	-	117

TABLE 1: Physical properties for giant elastocaloric compounds. Specific heat (C); Density (ρ); Temperature for the forward (cooling) transition (T_t); Transition strain (ε); Transition entropy change (ΔS_t), Adiabatic temperature change (ΔT_t) estimated from the transition entropy change, Transition temperature shift with uniaxial stress ($dT/d\sigma$); Minimum value of the applied stress ($\Delta\sigma$) to obtain reported entropy and temperature changes; Isothermal entropy change from indirect methods (ΔS^i), and estimated from measured temperature changes (ΔS^e) ; Adiabatic temperature change determined from direct measurements (ΔT^d), and estimated from the measured isothermal entropy change (ΔT^e). When not reported for the particular sample, specific heat and density values have been taken (or computed) for compounds with compositions close to the listed compound (the accuracy for these data is estimated to be ±10%) .

(*) Anomalously high C.

(#) Ill defined due to the existence of a critical point at around 300 MPa

Compound	Crystallographic change	C ($Jkg^{-1}K^{-1}$)	ρ (kgm^{-3})	T_t (K)	Δv/v %	ΔS_t ($Jkg^{-1}K^{-1}$)	ΔT_t (K)	dT/dp (10^{-3} $KMPa^{-1}$)	Δp (MPa)	ΔS^{qd} ($Jkg^{-1}K^{-1}$)	ΔT^{d} (K)	ΔT^{qd} (K)	ΔT^{e} (K)	Reference
$Fe_{49}Rh_{51}$	C(*Pm3m*)-C(*Pm3m*)	470	9800	310	1	12	8	59	250	12	-	9	8	74,74
$LaFe_{11.33}Co_{0.47}Si_{1.2}$	*C(Fm-3c)-C(Fm-3c)*	430	7200	250	1	11.4	6	-94	200	8.6	2.2	-	5	79
Mn_3GaN	C(*Pm-3m*)-C(*Pm-3m*)	450	6990	290	1	22	14	-65	140	22	1.3	4.5	14	80
$Gd_5Si_2Ge_2$	M($P112_1/a$)-O(*Pnma*)	300	7540	260	1	21	18	35	200	11	1	-	10	84
$MnCoGe_{0.99}In_{0.01}$	H($P6_3/mmc$)-O(*Pnma*)	450	7950	310	3.9	55	38	- 77	300	(52)	8.4	(18.5)	36	86
$(MnNiSi)_{0.62}(FeCoGe)_{0.38}$	H($P6_3/mmc$)-O(*Pnma*)	550	7300	338	4	62	38	-75	270	74	3	16	33	87
$Ni_{49.26}Mn_{36.08}In_{14.66}$	C(*Fm3m*) - T/M	400	8200	290	0.5	27	19	18	260	24	-	4.5	18	121
$Ni_{50}Mn_{33}In_{17}$	C(*Fm3m*) - T/M	400	8200	275	0.5	24	16	19	250	13	-	3	9	122
$Ni_{51}Mn_{33}In_{16}$	C(*Fm3m*) - T/M	400	8200	330	0.5	41	34	18	250	35	-	4	29	122
$Ni_{42.7}Co_{8.87}Mn_{31.67}Ga_{14.98}In_{2.01}$	C(*Fm3m*) - T/M	400	8000	400	0.7	21	21	30	250	16	-	-	16	124
$BaTiO_3$	C(*Pm-3m*)-T(*P4mm*)	500	6000	400	0.11	2.4	2	-55	100	1.6	-	1	2	127
$BaTiO_3$	T(*P4mm*)-O(Bmm2)	500	6000	280	0.03	2.0	1	-30	100	1.3	-	-	1	127
$PbTiO_3$	C(*Pm-3m*)-T(*P4mm*)	500	8740	770	0.4	27	41	-140	260	(2.7)	-	(1.9)	4	128
$(NH_4)_2SO_4$	O(*Pnam*) - O ($Pna2_1$)	1700	1770	220	1	130	17	- 50	100	60	-	-	8	131
$(NH_4)_2NbOF_5$	O($Cmc2_1$)-M(*C2*)-M(*Ia*)	1020	1450	260,220	0.2,0.3	155	39	-45	1000	(100)	-	(15)	25	133
$(NH_4)_2MoO_2F_4$	O(*Cmcm*)-O(*Pnma*)	1050	2580	270	0.2	83	21	93	900	(73)	-	(18)	18	134
$(NH_4)_2WO_2F_4$	O(*Cmcm*)-Tric(*P-1*)	850	3570	201	0.4	61	14	13	500	(40)	-	(14)	9	134
$(NH4)_2SnF_6$	Trig(*P-3m1*)-Tric(*P-1*)	570	2870	110	1	61	11	-157	100	(61)	-	(11)	11	135
Rb_2KTiOF_5	C(*Fm-3m*)- T(*I4/m*)	680	2560	215	1.2	69	22	110	600	(46)	-	(18)	15	136

TABLE 2: Physical properties for giant barocaloric compounds. Specific heat (C); Density (ρ); Temperature for the forward (cooling) transition (T_t); Relative volume change (Δv/v); Transition entropy change (ΔS_t), Adiabatic temperature change (ΔT_t), estimated from the transition entropy change; Transition temperature shift with pressure (dT/dp); Minimum value of the applied pressure (Δp) to obtain reported entropy and temperature changes; Isothermal entropy change from quasi-direct methods (ΔS^{qd}); Adiabatic temperature change determined from direct measurements (ΔT^{d}); quasi-direct measurements (ΔT^{qd}), and estimated from the measured isothermal entropy change (ΔT^{e}). When not reported for the particular sample, specific heat and density values have been taken (or computed) for compounds with compositions close to the listed compound (the accuracy for these data is estimated to be ±10%).

Values in bracket for ΔS^{qd} correspond to data obtained from improper quasi-direct methods (see text for details).

Click here to access/download

Production Data

zipped files.rar